International Journal of Heat and Mass Transfer 61 (2013) 226–244

Contents lists available at SciVerse ScienceDirect

International Journal of Heat and Mass Transfer

journal homepage: www.elsevier.com/locate/ijhmt

Forced convection from a circular cylinder in pulsating flow with and without the presence of porous media

Gazy F. Al-Sumaily [a,b,*], Mark C. Thompson [a]

[a] Fluids Laboratory for Aeronautical and Industrial Research (FLAIR), Department of Mechanical and Aerospace Engineering, Monash University, Victoria 3800, Australia
[b] Department of Mechanics and Equipments Engineering, University of Technology, Baghdad, Iraq

ARTICLE INFO

Article history:
Received 30 October 2012
Received in revised form 21 January 2013
Accepted 25 January 2013

Keywords:
Pulsating flow
Forced convection
Porous media
Non-Darcian effects
Local thermal non-equilibrium

ABSTRACT

This paper examines the changes to the flow and heat transfer induced by a non-zero mean sinusoidally varying flow past a cylinder. This is done by simulating steady and pulsatile forced convective flows over a circular cylinder placed in either a horizontal empty or a porous medium filled channel. The incompressible Navier–Stokes equations are used for the empty channel, and the Darcy–Brinkmann–Forchheimer momentum and the two-equation energy *LTNE* models in the porous-material filled channel. The effects of pulsation frequency *St* and amplitude *A* on heat transfer are quantified, as the Reynolds number (Re_D = 1–250) and type of porous material (k_r = 0.1, 1.0, 10, 100) are varied, whilst keeping the structural properties of the porous medium constant. In the empty (non-filled) channel, initially steady and then unsteady wakes evolve with an increase in Reynolds number. For the time-dependent case, two kinds of wake structure, namely fully periodic and quasi-periodic shedding, are observed depending on the values of Reynolds number, oscillation amplitude and forcing frequency. For the porous-medium filled channel simulations, a highly stable flows results, i.e., without forming extended wakes in the regions behind and in front of the cylinder, due to the damping from the porous medium. This is true even at high amplitudes, e.g., $A > 1.0$, which generates reverse flow in the channel. In general, using porous media promotes much higher heat transfer enhancement from the cylinder than that promoted by using pulsating flow, particularly at higher Reynolds number. But, a significant thermal benefit can be achieved by combining both schemes; however, only at the higher Reynolds numbers studied.

1. Introduction

There has been a growing need in many modern technological thermal applications for using highly effective cooling techniques to achieve a satisfactory heat transfer enhancement with a minimum frictional losses, including a variety of passive or active cooling techniques. Among the heat transfer enhancement schemes, one of the promising techniques is the use of porous media subjected to flow pulsation. Porous media has emerged as a convincing passive cooling enhancer due to its large contact surface area to volume ratio and intense mixing of fluid flow. Also, the forced pulsation of incoming fluid at the entrance of the channel is another active augmenting method due to the hydrodynamic instability in a shear layer, which substantially increases lateral, large-scale flow mixing and hence augments the convective thermal transports in the direction normal to the heated surface.

Generally, the research that has been done on oscillating flow with porous media is really scarce and incomplete. Efforts have been given to exploring the use of porous media as a heat sink in a confined channel subjected to a pulsating flow due to the increasing demand to achieve higher heat transfer removal from chips used in high-performance high-power electronic devices. These studies are related to the aspect of forced-pulsating convection flow over full- or partial-porous systems. Paek et al. [26] performed an experimental study of pulsating flow through an insulated horizontal packed bed of spherical beads. It is indicated that the heat transport from the porous material is little affected by the introduction of flow pulsation if the pulsating amplitude is small; however, the heat transfer is decreased when the amplitude becomes large enough to cause a backward flow. Also, for a given amplitude, the pulsating frequency shows a positive effect on the rate of heat transfer between the packed bed and the flowing fluid; yet, these rates are still less than that for the case of steady flow. Fu et al. [10] and Leong and Jin [22,23] reported the experimental results for heat transfer in porous channels subjected to steady and oscillating air flows with reticulated vitreous carbon and metal foam materials. They found that the length-averaged Nusselt number for oscillating flow is higher than that for steady flow. The effects

* Corresponding author at: Fluids Laboratory for Aeronautical and Industrial Research (FLAIR), Department of Mechanical and Aerospace Engineering, Monash University, Victoria 3800, Australia. Tel.: +61 3 9905 4000; fax: +61 3 9905 4007.
E-mail addresses: gazy.alsumaily@monash.edu (G.F. Al-Sumaily), mark.thompson@monash.edu (M.C. Thompson).

0017-9310/$ - see front matter © 2013 Elsevier Ltd. All rights reserved.
http://dx.doi.org/10.1016/j.ijheatmasstransfer.2013.01.067

Nomenclature

A	dimensionless oscillating amplitude of axial inlet velocity
a_{sf}	specific interfacial area (m^{-1})
Bi	Biot number, $Bi = h_{sf} a_{sf} D_{cy}^2 / k_s$.
c_p	specific heat capacity (J/kg K)
C_F	inertial coefficient, $C_F = 1.75/\sqrt{150\varepsilon^3}$
d_p	particle diameter (m)
D_{cy}	cylinder diameter (m)
Da	Darcy number, $Da = K/D_{cy}^2$
$\acute{f}$	pulsating frequency (Hz)
h_{cy}	cylinder surface heat transfer coefficient (W/m^2 K)
h_{sf}	interfacial heat transfer coefficient (W/m^2 K)
H	channel height (m)
k_d	dispersion thermal conductivity (W/m K)
k_f	fluid thermal conductivity (W/m K)
k_s	solid thermal conductivity (W/m K)
$k_s t$	stagnant thermal conductivity (W/m K)
k_r	solid/fluid thermal conductivity ratio, $k_r = k_s/k_f$
K	permeability of the porous medium, $K = \varepsilon^3 d_p^2/150(1-\varepsilon)^2$ (m^2)
L	channel length (m)
Nu	Nusselt number
$\acute{P}_f$	fluid pressure (N/m^2)
P_f	dimensionless fluid pressure, $P_f = \acute{P}_f/\rho_f \acute{u}_o^2$
Pr	Prandtl number, $Pr = \nu_f/\alpha_f$
Re_D	Reynolds number, $Re_D = \acute{u}_o \rho_f D_{cy}/\mu_f$
S	circumference of the cylinder (m)
St	dimensionless oscillating frequency parameter, Strouhal number, $\acute{f} D_{cy}/\acute{u}_o$
St_{res}	the resonant frequency
$\acute{t}$	time (s)
t	dimensionless time, $t = \acute{t}\acute{u}_o/D_{cy}$
$\acute{T}$	temperature (K)
$\acute{\mathbf{u}}$	vectorial fluid velocity (m/s)
$\mathbf{u}$	dimensionless vectorial fluid velocity, $\mathbf{u} = \acute{\mathbf{u}}/u_o$
$\acute{u}$	horizontal velocity component (m/s)
u	dimensionless horizontal velocity component, $u = \acute{u}/\acute{u}_o$
$\acute{u}_o$	horizontal fluid velocity at the inlet of the channel (m/s)
$\acute{v}$	vertical velocity component (m/s)
v	dimensionless vertical velocity component, $v = \acute{v}/\acute{u}_o$
$\acute{x}$, $\acute{y}$	horizontal and vertical coordinates (m)
x, y	dimensionless horizontal and vertical coordinates, $x = \acute{x}/D_{cy}$, $y = \acute{y}/D_{cy}$

Greek symbols

α_r	thermal diffusivity ratio, $\alpha_r = \alpha_s/\alpha_f$
ε	porosity
θ	dimensionless temperature, $\theta = (\acute{T} - \acute{T}_o)/(\acute{T}_h - \acute{T}_o)$
μ_f	fluid dynamic viscosity (kg/m s)
ρ_f	fluid density (kg/m^3)
ν_f	fluid kinematic viscosity (m^2/s)
φ	angular coordinate (°)

Subscripts

eff	effective
f	fluid
o	inlet of the channel
s	solid
t	total
w	wall of the channel

of thermal conductivity and permeability for different metal foam materials, and the kinetic Reynolds number based on the oscillating frequency and the amplitude, on heat transfer are also analyzed. It is shown that heat transfer from porous channel subjected to an pulsating flow can be enhanced by using materials of lower permeability and high thermal conductivity, and this enhancement increases with increasing the amplitude, and also with increasing the frequency but for relatively low values. Khodadadi [18] analyzed analytically a fully developed oscillatory flow through a porous medium channel bounded by two impermeable parallel plates, showing that the velocity profiles exhibit maxima next the wall. However, this study is not dealt with the issue of associated heat transports.

Numerically, Sozen and Vafai [28] simulated compressible flow of an ideal gas through an adiabatic packed bed. The effect of oscillating hydrodynamic and thermal inlet boundary conditions on the transport phenomena is examined. Once again, the average energy storage characteristics are found to be very close, without major differences, for both oscillating and constant boundary conditions. Another numerical data on heat transport of forced pulsating flow in a porous channel with a uniform temperature walls was provided by Kim et al. [19]. Their results show that the effect of pulsating on heat transfer between the channel wall and flowing fluid is more pronounced in the case of small pulsating frequency and large amplitude. Jue [14] tested oscillatory driven-cavity flow with mixed convection in a fluid-saturated porous medium. They found that the largest heat transfer occurs at a particular frequency which is known as the resonant frequency, and they also mentioned that the trend of the variation of heat transfer versus the oscillating frequency is seriously affected by Darcy number. Also, Huang and Yang [12] who examined fluid flow and thermal characteristics of oscillatory flow through a channel with two porous-block-mounted heat sources in tandem indicted to the presence of a critical value of Strouhal number (oscillating frequency) to obtain a maximum heat transfer enhancement factor. Below and above this critical value, the enhancement factor decreases afterward. This is occurred at low amplitude ($A = 0.6$). They also indicated to that the heat transfer enhancement factor for both heaters increases considerably with the pulsating amplitude. It is worth noting that their results show that the values of the pulsating heat transfer enhancement factor are not always larger than that of steady non-pulsating heat transfer enhancement factor depending on the values of the amplitude and frequency of the pulsating flow.

Steady and Pulsatile flow in a channel partially filled with two porous layers subjected to constant wall heat flux was also investigated numerically by Forooghi et al. [9]. Although, their results show the same finding for the pulsating amplitude which has a positive influence on heat transfer, entirely different trend of average Nusselt number against the Womersley number or frequency is observed. It has a minimum in a particular frequency, but surprisingly the maximum average Nusselt number occurs at the lowest frequency. This case is examined at high pulsating amplitude ($A = 1.5$). Therefore, from the above-mentioned studies, it seems that the influence of the pulsating frequency on heat transfer depends on the amplitude of pulsation. Such a finding would require further investigation since such observation has been not reported in the literature.

The problem of convective heat transfer over circular cylinder embedded in porous media has been the major topic for various studies in the past decades due to its relevance in a wide range of applications such as chemical catalytic reactors, nuclear waste repositories, solar power collectors, and heat exchangers. Most of these studies have been conducted on steady forced convection

flow past cylinder immersed in a porous material for heat transfer augmentation. Murty et al. [24] investigated the effect of Reynolds, Darcy, and Forchheimer numbers on forced convective heat released from a circular cylinder embedded in a porous medium. They concluded that the effect of inertial forces on the Nusselt number depends on the permeability of the porous medium used. Thevenin and Sadaoui [29] used the Darcy–Brinkmann model to investigate forced convective flow over a cylinder immersed in a fibrous porous medium for a range of Reynolds number 1–100 to avoid the influence of thermal dispersion. More than 80% heat transfer enhancement can be obtained from a single cylinder by immersing it in a porous medium at high Darcy number was concluded by Layeghi and Nouri-Borujerdi [20] who performed a heat transfer analysis for a single cylinder and an array of cylinders by using the Darcy and the Darcy–Brinkman models. The analysis was carried out with and without the presence of porous media at low Péclet number ($\leqslant$40) for a single cylinder, and at intermediate Péclet number ($\leqslant$300) for arrays of cylinders. Layeghi and Nouri-Borujerdi [21] numerically analyzed the steady-state of the problem in the range of Péclet number $\leqslant$40 with constant Prandtl number equal to 1.0, by using the simple Darcy model. The effect of porosity and permeability of the porous medium on the thermal field around the cylinder was examined.

Furthermore, Younis [35] also presented numerical results for forced convective cross-flow and heat transfer from a cylinder and a bundle of staggered cylinders, with and without a porous medium using the standard Navier–Stokes equations with the Darcy–Brinkmann model. The focus was on the effects of the permeability and the thermal conductivity of the porous material on the fluid flow and the rate of heat transfer from a heated cylinder. The results for bare cylinders without porous media were compared with those for cylinders embedded in a porous medium. It was found that it is possible to enhance the heat transfer rate from a cylinder placed in a cross-flow by several fold using a porous medium with high permeability and high thermal conductivity. Younis and Mohamad [36] also used the Darcy–Brinkmann model to study fluid dynamics and heat transfer for flow over a heated cylinder immersed in an air-saturated porous medium. They investigated the effect of the presence of porous media on Von Karman vortex shedding formation at the cylinder wake, and on the heat transfer enhancement. Interestingly, their results showed that the Von Karman Vortex periodic shedding (Two-counter rotating vortices) can be formed behind the cylinder in a high permeable porous medium, i.e., Darcy number $Da = 0.01$, at Reynolds number $Re = 200$, which changes to a steady wake by decreasing the permeability to $Da = 0.005$, and suppresses completely at $Da = 0.001$. Also, it was predicted that the porous medium enhances the rate of heat transfer, and the rate of enhancement increases by using a porous medium with higher thermal conductivity and lower permeability. By using the local thermal non-equilibrium (*LTNE*) energy model, Rees et al. [27] and Wong et al. [34] demonstrated how the thermal fields of the solid and fluid phases, and the rate of heat transfer around and from a horizontal circular cylinder, are affected by the removing the local thermal equilibrium (*LTE*) condition.

To the authors' knowledge, although the literature reveals that there is only one study done by Iwai et al. [13] to examine the fluid flow and heat transfer characteristics of a circular cylinder mounted inside an empty (non-filled) horizontal channel and exposed to an oscillatory flow, this problem with the presence of porous media have been not investigated to the recent date. Therefore, the main purpose of the present study is to fill this gap. In this article, steady and non-zero mean pulsatile flow and heat transfer over a cylinder placed in a plate channel with and without the presence of porous media are numerically investigated under the *LTNE* condition. As the first objective of this work, the change in heat transfer when a harmonic term is superimposed on the steady state inlet velocity in both empty and porous channels is studied. The effect of amplitude and frequency of pulsation on heat transfer is thoroughly examined. The second objective is to find out the reason for the contradictory conclusions in the studies of Huang and Yang [12] and Forooghi et al. [9] concering the effect of pulsation frequency on heat transfer. Also, a briefly investigation will be performed to examine the sensibility of heat transfer to the thermophysical, i.e., solid/fluid thermal conductivity ratio, properties of the porous medium under the pulsatile flow.

2. Mathematical formulation

2.1. Statement of the problem

The problem considered in this study can be broadly categorised as predicting the flow and forced convection heat transfer from a single circular cylinder mounted in a two-dimensional empty (non-filled) channel or containing porous media, under steady or non-zero mean pulsatile upstream flow. The schematic diagrams of the cases considered are provided in Fig. 1. The cylinder is assumed to be isothermally heated at a constant temperature T_h' and cooled by the incoming external flow at T_o'. The confining horizontal walls have the same temperature T_w' as the flow at the inlet. The geometrical relationships are set as follows: The blockage ratio of the channel is $D_{cy}/H = 0.25$, where D_{cy} is the cylinder diameter, which is considered to be the unit scale length in the present study, and H is the channel height. The extent of the channel in the z-direction is assumed to be large enough so that the problem will essentially be two-dimensional. The sectionally-averaged velocity oscillates sinusoidally around the temporally-averaged flow velocity, at a period τ and an amplitude A. The inlet flow produces the same net mass flow; thus the steady flow can be thought of as either a temporal average of the pulsatile flow, or as a limiting case of when the pulsation amplitude approaches zero. The character of a pulsating flow is specified by two non-dimensional parameters. These are the pulsation frequency represented by the Strouhal number $St = f' D_{cy}/u_o'$, where $f' = 1/\tau$ is the forcing frequency and the velocity perturbation amplitude A. The study reports on cases with and without the presence of porous media.

2.2. Governing equations

Prior to analysing these cases, it is useful to state the assumptions on which the governing equations are based:

1. The fluid flow is laminar and incompressible.
2. Forced convection dominates the thermal field of the channels, i.e., natural convection effects can be ignored.
3. The fluid passing through the channels is Newtonian.
4. The porous medium is homogenous and isotropic.
5. The variation of thermo-physical properties of the fluid and solid phases with temperature can be neglected.
6. Interfacial radiation heat transfer in the porous channel can be ignored.
7. No heat generation occurs inside the porous medium.
8. But, importantly, local thermal equilibrium between the two phases is not assumed.

Taking in account these assumptions, the system of the governing equations of the continuity, momentum and energy, that predicts the flow and thermal fields in the porous channel, can be presented in the following vectorial form as given in Kaviany

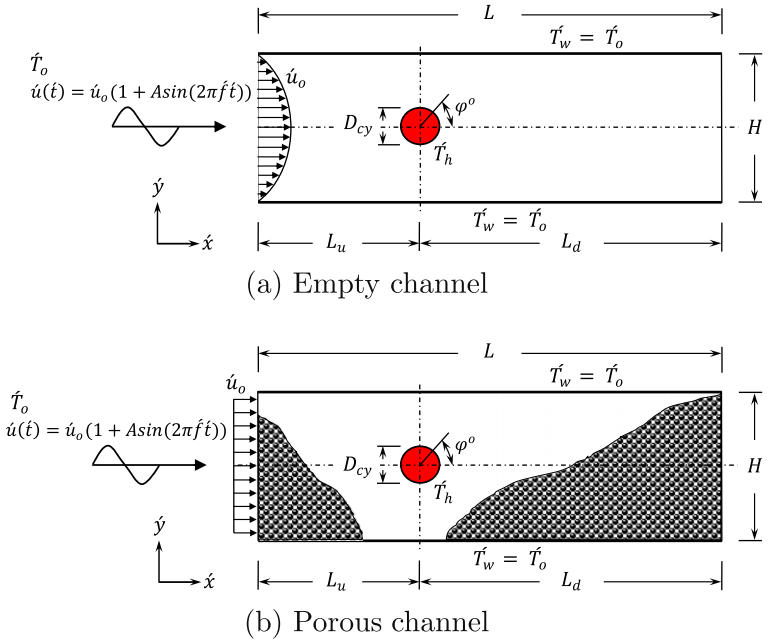

Fig. 1. Schematic diagram of a single heated circular cylinder mounted in a horizontal, (a) empty (non-filled), and (b) porous, channels subjected to a steady or pulsatile flow.

[17] and Nield and Bejan [25], based on the volume-average method:

$$\nabla \cdot \langle \acute{\mathbf{u}} \rangle = 0, \tag{1}$$

$$\frac{\rho_f}{\varepsilon}\left[\frac{\partial \langle \acute{\mathbf{u}} \rangle}{\partial \acute{t}} + \frac{1}{\varepsilon}\langle (\acute{\mathbf{u}} \cdot \nabla)\acute{\mathbf{u}} \rangle\right] = -\frac{\mu_f}{K}\langle \acute{\mathbf{u}} \rangle - \frac{\rho_f C_F}{\sqrt{K}}|\langle \acute{\mathbf{u}} \rangle|\langle \acute{\mathbf{u}} \rangle + \frac{\mu_f}{\varepsilon}\nabla^2 \langle \acute{\mathbf{u}} \rangle - \nabla \langle \acute{P}_f \rangle, \tag{2}$$

$$\varepsilon(\rho c_p)_f\left[\frac{\partial \langle \acute{T}_f \rangle}{\partial \acute{t}} + \langle \acute{\mathbf{u}} \rangle \cdot \nabla \langle \acute{T}_f \rangle\right] = \nabla \cdot [k_{f.\mathrm{eff},(x,y)} \nabla \langle \acute{T}_f \rangle] + h_{sf} a_{sf}(\langle \acute{T}_s \rangle - \langle \acute{T}_f \rangle), \tag{3}$$

$$(1-\varepsilon)(\rho c_p)_s \frac{\partial \langle \acute{T}_s \rangle}{\partial \acute{t}} = \nabla \cdot [k_{s.\mathrm{eff}} \nabla \langle \acute{T}_s \rangle] - h_{sf} a_{sf}(\langle \acute{T}_s \rangle - \langle \acute{T}_f \rangle), \tag{4}$$

where,

$$|\langle \acute{\mathbf{u}} \rangle| = \sqrt{\langle \acute{u}^2 \rangle + \langle \acute{v}^2 \rangle}, \tag{5}$$

Here, $\acute{\mathbf{u}}$ is the velocity vector field, $\acute{t}$ is the time variable, $\acute{P}_f$ is the pressure field and $\acute{T}$ is the temperature field. Subscripts f and s denote the fluid and solid phases, respectively, and eff refers to the effective property. The following are other fluid and medium properties: K is the permeability, C_F the inertia coefficient, μ_f the fluid dynamic viscosity, ρ the density, c_p the specific heat, ε the porosity, k the thermal conductivity, a_{sf} the specific surface area of the packed bed and h_{sf} the interfacial heat transfer coefficient. In addition, the primes refer to dimensional quantities and the operator $\langle \ldots \rangle$ denotes local volume average of a quantity.

In the momentum Eq. (2), the first term on the right-hand side represents the frictional resistance due to the presence of the micro-pore structure, while the square term, the second term on the right-hand side, is caused by the inertial effects from passing through the solid matrix. The third term on the right-hand side accounts for the effect of friction posed by an external boundary on the flow. With regard to the energy equations, it can be seen that as the solid phase is stationary, the energy transport through the solid phase, i.e., Eq. (4), only needs to account for conduction. However, an additional mode of heat transfer emerges if there is a difference in the temperature distributions between the fluid and solid phases. This transfer mode can be conceived of as convective heat transfer that can be formulated via a solid-to-fluid heat transfer coefficient h_{sf}.

After introducing the dimensionless variables defined in the following:

$$x, y = \frac{\acute{x}, \acute{y}}{D_{cy}}, \quad \langle \mathbf{u} \rangle = \frac{\langle \acute{\mathbf{u}} \rangle}{\acute{u}_o}, \quad t = \frac{\acute{t}\acute{u}_o}{D_{cy}}, \quad \langle \theta \rangle = \frac{\langle \acute{T} \rangle - \acute{T}_o}{(\acute{T}_h - \acute{T}_o)}, \quad \langle P_f \rangle = \frac{\langle \acute{P}_f \rangle}{\rho_f \acute{u}_o^2}. \tag{6}$$

The governing equations can be transformed into a non-dimensional following form:

$$\nabla \cdot \langle \mathbf{u} \rangle = 0, \tag{7}$$

$$\frac{1}{\varepsilon}\left[\frac{\partial \langle \mathbf{u} \rangle}{\partial t} + \frac{1}{\varepsilon}\langle (\mathbf{u} \cdot \nabla)\mathbf{u} \rangle\right] = -\frac{1}{Re_D Da}\langle \mathbf{u} \rangle - \frac{C_F \varepsilon}{\sqrt{Da}}|\langle \mathbf{u} \rangle|\langle \mathbf{u} \rangle + \frac{1}{\varepsilon Re_D}\nabla^2 \langle \mathbf{u} \rangle - \nabla \langle P_f \rangle, \tag{8}$$

$$\frac{\varepsilon}{k_r}\left[\frac{\partial \langle \theta_f \rangle}{\partial t} + \langle \mathbf{u} \rangle \cdot \nabla \langle \theta_f \rangle\right] = \frac{1}{Re_D Prk_r}\nabla \cdot \left[\frac{k_{f.\mathrm{eff},(x,y)}}{k_f}\nabla \langle \theta_f \rangle\right] + \frac{Bi}{Re_D Pr}(\langle \theta_s \rangle - \langle \theta_f \rangle), \tag{9}$$

$$\frac{(1-\varepsilon)}{\alpha_r}\frac{\partial \langle \theta_s \rangle}{\partial t} = \frac{1}{Re_D Pr}\nabla \cdot \left[\frac{k_{s.\mathrm{eff}}}{k_s}\nabla \langle \theta_s \rangle\right] - \frac{Bi}{Re_D Pr}(\langle \theta_s \rangle - \langle \theta_f \rangle). \tag{10}$$

Here, k_r and α_r are the solid-to-fluid thermal conductivity and diffusivity ratios, k_s/k_f and α_s/α_f, respectively. In addition, the key dimensionless groups appearing in these equations are: the Reynolds, Darcy, Prandtl, and Biot numbers:

$$Re_D = \frac{\acute{u}_o D_{cy} \rho_f}{\mu_f}, \quad Da = \frac{K}{D_{cy}^2}, \quad Pr = \frac{\nu_f}{\alpha_f}, \quad Bi = \frac{D_{cy}^2 h_{sf} a_{sf}}{k_s}. \tag{11}$$

In the empty channel, the dimensionless momentum Eq. (8) allows for a smooth transition between fluid flow through porous media and the Navier–Stokes equations in a space without porous media by taking $\varepsilon = 1$ and $K \to \infty$. Also, the fluid phase energy

Table 1
Four physical domains chosen, with their upstream and downstream lengths, and the total number of macro-elements and nodes.

Domain	L_u	L_d	Macro-elements	Macro-nodes
$M1$	$3D_{cy}$	$10D_{cy}$	670	615
$M2$	$5D_{cy}$	$12D_{cy}$	742	683
$M3$	$8D_{cy}$	$15D_{cy}$	850	785
$M4$	$8D_{cy}$	$20D_{cy}$	940	870

model (9) can be transformed to the standard fluid energy equation by taking $k_{f.eff} = k_f$ and $Bi = 0$ to predict the fluid thermal field in the absence of porous media.

The empirical expression suggested by Dullien [5] for the specific surface area of the packed bed a_{sf} is employed in the present investigation as follows:

$$a_{sf} = \frac{6(1-\varepsilon)}{d_p}, \tag{12}$$

where, d_p is the particle diameter. While, the formulation of the interfacial heat transfer coefficient h_{sf} is based on the empirical correlation proposed by Wakao et al. [32] for packed beds and can be expressed as:

$$h_{sf} = \frac{k_f}{d_p}\left[2 + Pr^{1/3}Re_p^{0.6}\right], \tag{13}$$

where, Re_p is the *particle Reynolds number*

$$Re_p = \frac{\rho_f |\langle \mathbf{u} \rangle| d_p}{\mu_f}. \tag{14}$$

In turn, this allows the *Biot number* to be expressed as

$$Bi = 6(1-\varepsilon)\left(\frac{1}{k_r}\right)\left(\frac{D_{cy}}{d_p}\right)^2\left[2 + Pr^{1/3}Re_p^{0.6}\right]. \tag{15}$$

The permeability of the porous medium K incorporated in the Darcy number and the inertia coefficient C_F, in the momentum Eq. (8), are inherently tied to the structure of the porous medium. These are generally based on empirical fits from experimental findings, i.e., no universal representations exist. For a randomly packed bed of spheres such coefficients were reported by Ergun [6], and were expressed in terms of porosity ε and particle diameter d_p as follows:

$$K = \frac{\varepsilon^3 d_p^2}{150(1-\varepsilon)^2}, \tag{16}$$

$$C_F = \frac{1.75}{\sqrt{150\varepsilon^3}}. \tag{17}$$

The effective thermal conductivity of the fluid phase $k_{f.\mathrm{eff}}$ is composed of a sum of the stagnant k_{st} and dispersion k_d conductivities:

$$k_{f.\mathrm{eff},\langle x,y \rangle} = k_{st} + k_{d\langle x,y \rangle}. \tag{18}$$

Typically, the stagnant conductivity is the product of the phase fractions and the individual thermal conductivities of the fluid and the solid phases. In the ongoing investigation, the semi-theoretical model of Zehner and Schluender [37] for calculating the stagnant conductivity is used:

Table 2
Domain size study for a steady forced convective flow in two; (a) empty, and (b) porous, channels for two values of $Re_D = 10$ and 250, with order of polynomial $p = 6$.

Domain	(a) Empty channel		(b) Porous channel			
	$Re_D = 10$	$Re_D = 250$	$Re_D = 10$		$Re_D = 250$	
	Nu_f	Nu_f	Nu_f	Nu_s	Nu_f	Nu_s
$M1$	5.057827	19.441979	7.984645	0.129630	69.705124	0.130727
$M2$	5.122665	19.539155	7.968639	0.128593	69.699884	0.129716
$M3$	5.153913	19.660151	7.965108	0.128553	69.698501	0.129681
$M4$	5.153913	19.660764	7.965108	0.128553	69.698501	0.129681

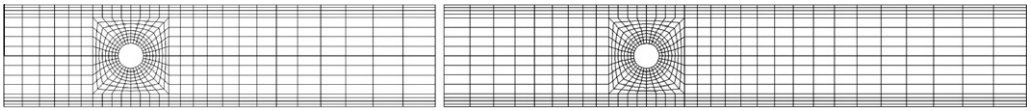

Fig. 2. Typical computational macro-meshes for the; (Left) $M2$ physical domain used for steady flow in the porous channel, and (Right) $M3$ physical domain used for steady flow in the empty channel.

Table 3
Study the effect of upstream length of the $M2$ domain allocated for the porous channel, subjected to a non-zero pulsatile flow at its highest amplitude $A = 3.0$, on Nu_f and Nu_s, at (a) $Re_D = 1.0$ and (b) 250, and for two minimum and maximum frequency limitations $St = 0.1$ and 2.0.

L_u	$Re_D = 1.0$				$Re_D = 250$			
	$f = 0.1$		$f = 2.0$		$f = 0.1$		$f = 2.0$	
	Nu_f	Nu_s	Nu_f	Nu_s	Nu_f	Nu_s	Nu_f	Nu_s
$5D_{cy}$	2.79191	0.19102	2.47771	0.18740	72.00615	0.29049	68.31169	0.30137
$6D_{cy}$	2.75971	0.18934	2.47775	0.18740	71.12894	0.28907	68.31170	0.30137
$7D_{cy}$	2.74269	0.18845	2.47772	0.18740	71.02395	0.28889	68.31171	0.30137
$8D_{cy}$	2.73718	0.18814	2.47773	0.18740	71.02322	0.28889	68.31172	0.30137
$9D_{cy}$	2.73495	0.18804	2.47773	0.18740	71.02282	0.28889	68.31172	0.30137
$10D_{cy}$	2.73470	0.18803	2.47773	0.18740	71.02238	0.28889	68.31172	0.30137

Table 4
Study the effect of upstream length of the *M*3 domain allocated for the empty channel, subjected to a non-zero pulsatile flow at its highest amplitude $A = 0.7$, on Nu_f, at $Re_D = 1.0$ and 250, and for two minimum and maximum frequency limitations $St = 0.1$ and 2.0.

Lu	$Re_D = 1.0$		$Re_D = 250$	
	$St = 0.1$	$St = 2.0$	$St = 0.1$	$St = 2.0$
	Nu_f	Nu_f	Nu_f	Nu_f
$8D_{cy}$	2.328386	2.381161	24.002609	24.374326
$9D_{cy}$	2.328386	2.381161	24.002609	24.374326
$10D_{cy}$	2.328386	2.381161	24.002609	24.374326
$11D_{cy}$	2.328386	2.381161	24.002609	24.374326
$12D_{cy}$	2.328386	2.381161	24.002609	24.374326

$$\frac{k_{st}}{k_f} = (1-\sqrt{1-\varepsilon}) + \frac{2\sqrt{1-\varepsilon}}{1-\lambda B} \times \left[\frac{(1-\lambda)B}{(1-\lambda B)^2}\ln(\lambda B) - \frac{B+1}{2} - \frac{B-1}{1-\lambda B}\right], \tag{19}$$

where $\lambda = 1/k_r$, and $B = 1.25[(1-\varepsilon)/\varepsilon]^{\frac{10}{9}}$. Whereas, the dispersion conductivity that incorporates the additional thermal transport due to the fluid's tortuous path around the solid particles is determined in both longitudinal and lateral directions based on the experimental correlation reported by Wakao and Kaguei [31], and is given by:

$$\frac{k_{dx}}{k_f} = 0.5\,Pr\,Re_p, \tag{20}$$

$$\frac{k_{dy}}{k_f} = 0.1\,Pr\,Re_p. \tag{21}$$

While, the effective thermal conductivity for the solid phase consists merely of the phase fraction component which is the stagnant component since the solid phase is stationary:

$$k_{s.\text{eff}} = (1-\varepsilon)k_s. \tag{22}$$

Heat transfer characteristics are evaluated based on the time-mean local and average Nusselt numbers along the heated surface of the cylinder. The Nusselt number is defined for the fluid and solid phases separately and is expressed as:

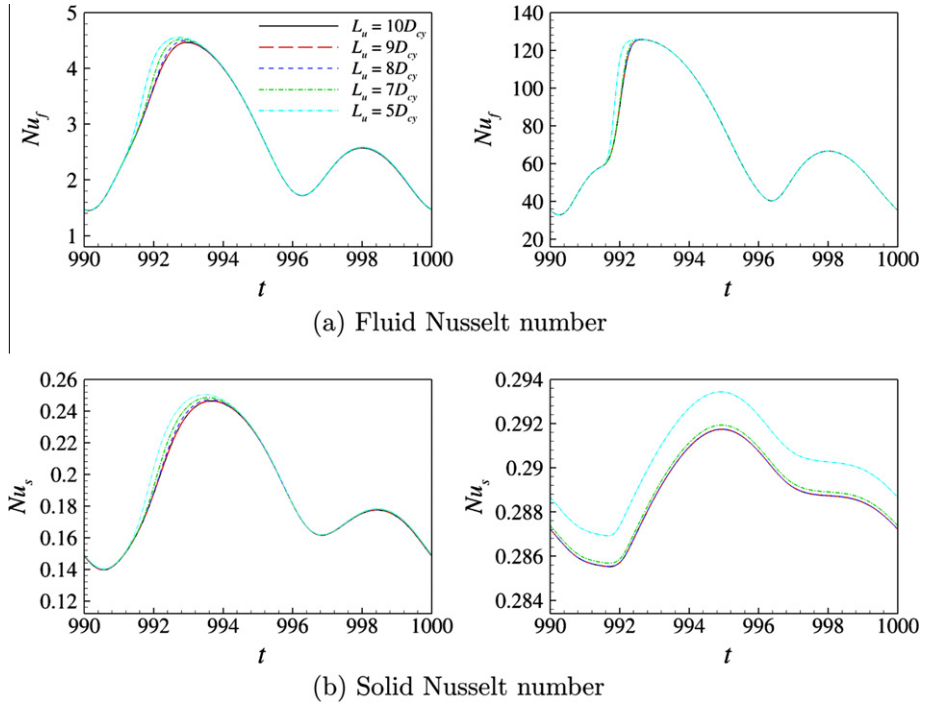

Fig. 3. The effect of upstream length L_u of the *M*2 domain for the porous channel under a non-zero pulsatile flow with amplitude $A = 3.0$ and frequency $St = 0.1$, on the transient variation of; (a) Nu_f, and (b) Nu_s for a one period, at (Left) $Re_D = 1.0$ and (Right) $Re_D = 250$.

Table 5
Grid resolution study of the computational domain *M2* for a single cylinder embedded in a horizontal porous channel, at two minimum and maximum values of solid-to-fluid thermal conductivity ratio $k_r = 0.01$ and 1000, and at two lowest and highest values of Reynolds number $Re_D = 1.0$ and 250. This is done by varying the interpolation polynomial order *p* within the range 2–8, while keeping the macro-element layout the same.

p	$Re_D = 1.0$				$Re_D = 250$			
	$k_r = 0.01$		$k_r = 1000$		$k_r = 0.01$		$k_r = 1000$	
	Nu_f	Nu_s	Nu_f	Nu_s	Nu_f	Nu_s	Nu_f	Nu_s
2	2.093937	0.208724	1.945964	0.124746	66.31117	0.303586	54.95857	0.260723
3	2.084829	0.208389	1.940192	0.124378	65.98328	0.302715	54.71937	0.259967
4	2.082658	0.208095	1.935207	0.124058	65.99555	0.302373	54.74098	0.259612
5	2.081221	0.207893	1.931993	0.123852	65.99180	0.302171	54.74359	0.259411
6	2.080121	0.207749	1.929790	0.123711	65.97858	0.302032	54.73227	0.259271
7	2.079330	0.207646	1.928184	0.123608	65.96869	0.301929	54.72206	0.259169
8	2.078717	0.207566	1.926967	0.123529	65.96135	0.301852	54.71413	0.259092

Table 6
Grid resolution study of the computational domain *M*3 for a single cylinder placed in a horizontal empty channel, at two lowest and highest values of Reynolds number Re_D = 1.0 and 250. This is done by varying the interpolation polynomial order *p* within the range 2–8, while keeping the macro-element layout the same.

p	Re_D = 1.0 Nu_f	Re_D = 250 Nu_f
2	2.086845	22.453573
3	2.084753	19.399868
4	2.082221	18.992643
5	2.080529	19.377584
6	2.079362	19.465532
7	2.078513	19.435192
8	2.077858	19.425336

Fluid phase local and average Nusselt numbers:

$$Nu_{f\varphi} = \frac{h_{cy}D_{cy}}{k_f} = \frac{-k_{f.\mathrm{eff}}[\partial\langle \acute{T}_f\rangle/\partial\mathbf{n}]D_{cy}}{k_f(\acute{T}_h - \acute{T}_o)}, \quad Nu_f = \frac{1}{S}\int_0^{\mathbf{s}} Nu_{f\varphi}\mathbf{ds}. \tag{23}$$

Solid phase local and average Nusselt numbers:

$$Nu_{s\varphi} = \frac{h_{cy}D_{cy}}{k_s} = \frac{-k_{s.\mathrm{eff}}[\partial\langle \acute{T}_s\rangle/\partial\mathbf{n}]D_{cy}}{k_s(\acute{T}_h - \acute{T}_o)}, \quad Nu_s = \frac{1}{S}\int_0^{\mathbf{s}} Nu_{s\varphi}\mathbf{ds}, \tag{24}$$

where **n** and **s** denote to the normal and tangential directions at the cylinder surface, respectively, and *S* is the circumference of the cylinder. Consequently, the time-mean average total Nusselt number Nu_t is defined as the summation of Nu_f and Nu_s:

$$Nu_t = Nu_f + Nu_s. \tag{25}$$

2.3. Boundary conditions

The problem is not completely specified without the provision of proper boundary conditions. In the problem under investigation Dirichlet boundary conditions, for the pertinent hydrodynamic and thermal variables, i.e., the velocity and temperature fields, are imposed at the inlet and solid boundaries. For example, the cylinder surface and the channel walls are maintained at constant temperatures, and a no-slip boundary condition is imposed at the cylinder surface and the confining walls. In addition, both fluid and solid phases are at the same temperature at the inlet of the

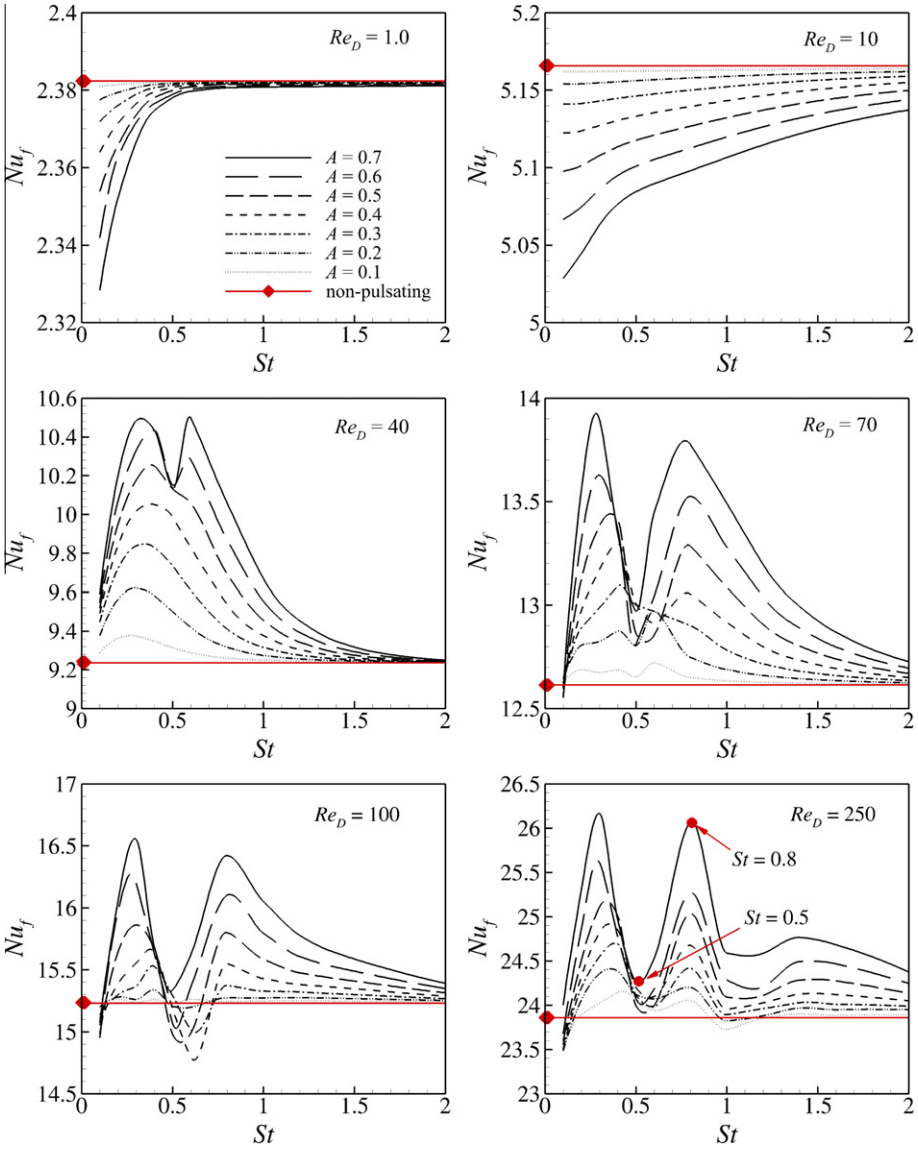

Fig. 4. Effect of pulsation frequency represented by Strouhal number, $0.1 \leqslant St \leqslant 2.0$, and amplitude $0.1 \leqslant A \leqslant 0.7$, on the fluid Nusselt number Nu_f from a cylinder placed in an empty plate channel under non-zero pulsatile flow, at different Re_D = 1.0, 10, 40, 70, 100 and 250.

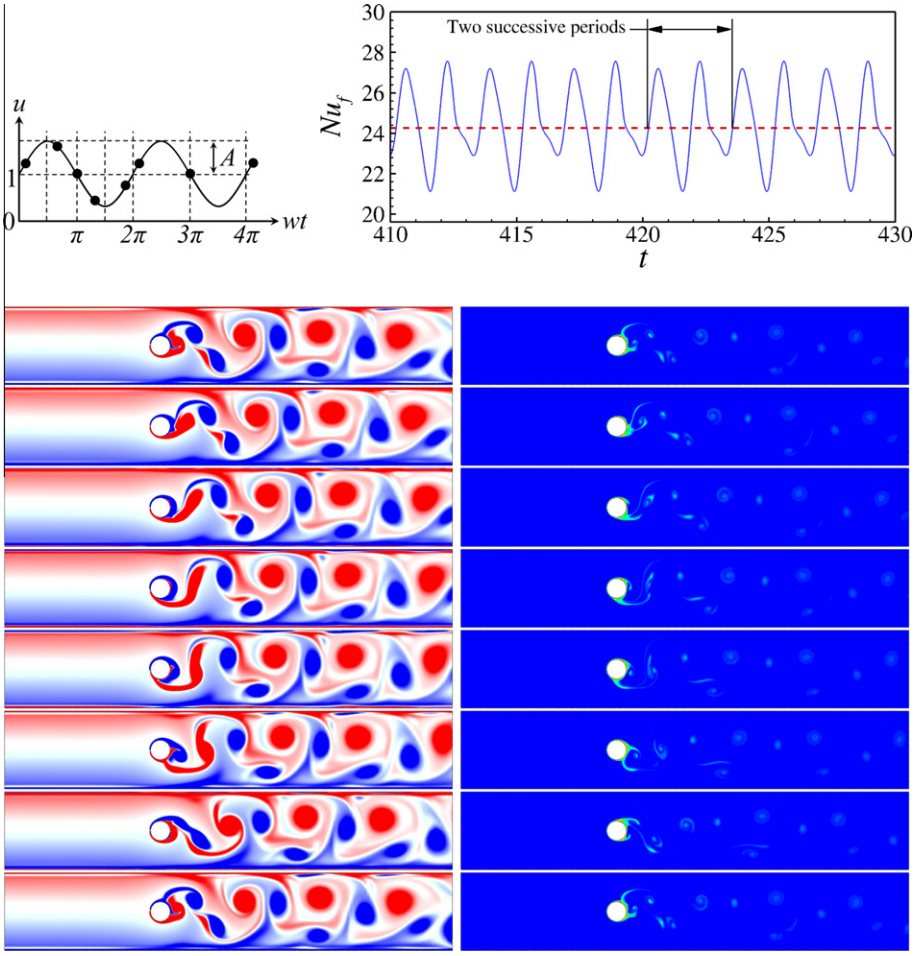

Fig. 5. Evolution of the flow and temperature fields represented by vorticity (Left) and isotherms (Right), respectively, at eight instants $wt = \pi/5, 3\pi/5, \pi, 7\pi/5, 9\pi/5, 11\pi/5, 3\pi$ and 4π, during two pulsation cycles, around a circular cylinder mounted in a horizontal empty channel exposed to a non-zero pulsatile flow, at $Re_D = 250$, Strouhal number $St = 0.5$ and pulsation amplitude $A = 0.7$. Positive (negative) vorticity and hot (cold) temperatures are represented by red (blue) contours, with ranges of $(-2,2)$ and $(0,1)$, respectively. The plot in the right top corner illustrates the oscillation of Nu_f from the cylinder over time, and the plot in the left top corner illustrates the inlet velocity waveform for pulsatile flow. (For interpretation of the references to color in this figure legend, the reader is referred to the web version of this article.)

channel. At the exit, Neumann boundary conditions are imposed on the normal velocity and the solid and fluid temperatures. In addition, the pressure is set to zero at the outlet boundary. At other boundaries the pressure satisfies a Neumann condition obtained by taking the dot-product of the momentum equation and Navier–Stokes equations with the surface normal vector. This higher-order boundary condition also ensures mass conservation at solid boundaries Karniadakis et al. [15]. Thus, the dimensional initial and boundary conditions can be mathematically expressed as:

$$
\begin{aligned}
&\text{at } \acute{t} = 0: \quad \langle \acute{u} \rangle = \langle \acute{v} \rangle = \langle \acute{T}_f \rangle = \langle \acute{T}_s \rangle = 0 \\
&\text{at } \acute{t} > 0: \quad \textbf{at inlet} \qquad (\acute{x} = 0,\ 0 < \acute{y} < H) \\
&\langle \acute{u} \rangle = \acute{u_o} \ \text{(for steady flow)} \\
&\langle \acute{u}(\acute{t}) \rangle = \acute{u_o}(1 + A\sin(2\pi \acute{f} \acute{t})) \qquad \text{(for pulsatile flow)} \\
&\langle \acute{v} \rangle = 0, \quad \langle \acute{T}_f \rangle = \langle \acute{T}_s \rangle = \acute{T_o} \\
&\textbf{at outlet} \qquad (\acute{x} = L,\ 0 < \acute{y} < H) \\
&\frac{\partial \langle \acute{u} \rangle}{\partial \acute{x}} = \frac{\partial \langle \acute{T}_f \rangle}{\partial \acute{x}} = \frac{\partial \langle \acute{T}_s \rangle}{\partial \acute{x}} = \langle \acute{v} \rangle = 0 \\
&\textbf{at the walls} \qquad (0 < \acute{x} < L,\ \acute{y} = 0 \text{ and } H) \\
&\langle \acute{u} \rangle = \langle \acute{v} \rangle = 0, \quad \langle \acute{T}_f \rangle = \langle \acute{T}_s \rangle = \acute{T_w} \\
&\textbf{at the cylinder boundary} \qquad (0 < \varphi^\circ < 360) \\
&\langle \acute{u} \rangle = \langle \acute{v} \rangle = 0, \quad \langle \acute{T}_f \rangle = \langle \acute{T}_s \rangle = \acute{T_h}.
\end{aligned}
\tag{26}
$$

By using the dimensionless variables in Eq. (6), the dimensionless initial and boundary conditions become as follows:

$$
\begin{aligned}
&\text{at } t = 0: \quad \langle u \rangle = \langle v \rangle = \langle \theta_f \rangle = \langle \theta_s \rangle = 0 \\
&\text{at } t > 0: \quad \textbf{at inlet} \qquad (x = 0, 0 < y < H/D_{cy}) \\
&\langle u \rangle = 1 \quad \text{(for steady flow)} \\
&\langle u(t) \rangle = 1 + A\sin(2\pi St\ t) \quad \text{(for pulsatile flow)} \\
&\langle v \rangle = \langle \theta_f \rangle = \langle \theta_s \rangle = 0 \\
&\textbf{at outlet} \qquad (x = L/D_{cy},\ 0 < y < H/D_{cy}) \\
&\frac{\partial \langle u \rangle}{\partial x} = \frac{\partial \langle \theta_f \rangle}{\partial x} = \frac{\partial \langle \theta_s \rangle}{\partial x} = \langle v \rangle = 0 \\
&\textbf{at the walls} \qquad (0 < x < L/D_{cy},\ y = 0 \text{ and } H/D_{cy}) \\
&\langle u \rangle = \langle v \rangle = \langle \theta_f \rangle = \langle \theta_s \rangle = 0 \\
&\textbf{at the cylinder boundary} \qquad (0 < \varphi^\circ < 360) \\
&\langle u \rangle = \langle v \rangle = 0, \quad \langle \theta_f \rangle = \langle \theta_s \rangle = 1.
\end{aligned}
\tag{27}
$$

For these boundary conditions, the fluid is assumed to enter the empty channel with a parabolic velocity profile, $u_o = u_{max}[y - (y/(H/2))^2]$, where, u_{max} is the maximum velocity in the channel, for both steady and pulsatile flows. In addition, in the porous channel the thermal equilibrium assumption is imposed at heated

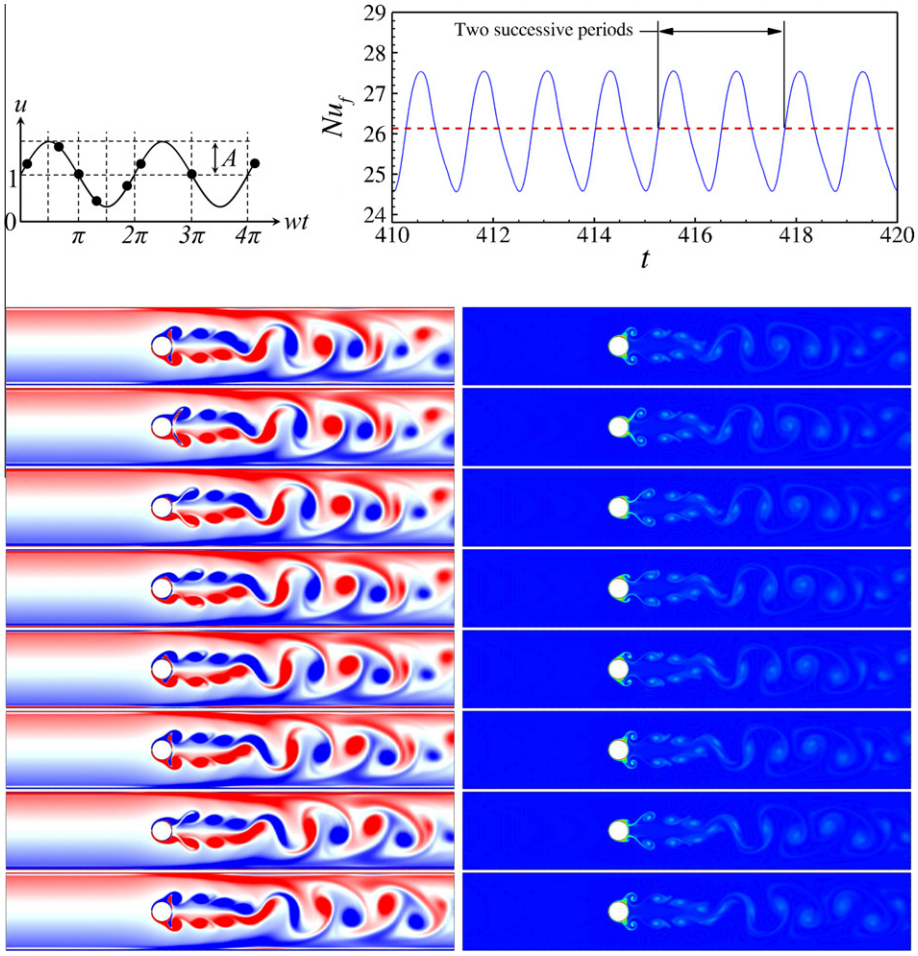

Fig. 6. Evolution of the flow and temperature fields represented by vorticity (Left) and isotherms (Right), respectively, at eight instants $wt = \pi/5, 3\pi/5, \pi, 7\pi/5, 9\pi/5, 11\pi/5, 3\pi$ and 4π, during two pulsation cycles, around a circular cylinder mounted in a horizontal empty channel exposed to a non-zero pulsatile flow, at $Re_D = 250$, Strouhal number $St = 0.8$ and pulsation amplitude $A = 0.7$. Positive (negative) vorticity and hot (cold) temperatures are represented by red (blue) contours, with ranges of $(-2,2)$ and $(0,1)$, respectively. The plot in the right top corner illustrates the oscillation of Nu_f from the cylinder over time, and the plot in the left top corner illustrates the inlet velocity waveform for pulsatile flow. (For interpretation of the references to colour in this figure legend, the reader is referred to the web version of this article.)

boundaries, e.g., the fluid and solid phases have the same temperature as that of the isothermal cylinder's surface, see Alazmi and Vafai [3] and Wong and Saeid [33].

3. Numerical method of solution

The above Eqs. (7)–(10) form the mathematical model for analysing the transient momentum and energy transport in unsteady forced convective flow in a porous media. This is a system of highly coupled equations describing the evolution of the four pertinent fields, i.e., velocity $\langle \mathbf{u} \rangle$, fluid temperature $\langle \theta_f \rangle$, solid temperature $\langle \theta_s \rangle$ and pressure $\langle P_f \rangle$. To numerically solve this system of equations, it is necessary to discretise the problem in both time and space.

The temporal discretisation method used for this study is a two- and three-step time-splitting scheme for the energy and momentum equations, respectively. The name of time-splitting for this method is because the right-hand side of the equations is divided into two or three groups, and integrated separately, which results in the overall integration over one time-step being split into two or three sub-steps. The method is thoroughly described in Chorin [4], Karniadakis et al. [15] and Thompson et al. [30].

The nodal-based spectral-element method, which is a high-order Galerkin finite-element approach, is implemented to discretise the governing equations in space. In this method, the computational domain is usually subdivided coarsely into a series of discrete macro-elements. The spatial discretisation employed here is based on quadrilateral elements, although these elements are free to have curved sides. This method employs tensor-product Lagrange polynomials, associated with Gauss–Legendre–Lobatto quadrature points, as shape functions over each quadrilateral element. Refinement (spatial resolution) can be made to the generated macro-mesh by either changing the number of quadrilateral elements (h-refinement), particularly in regions of the domain that experience high gradients, or by changing the order of the Lagrange polynomial shape functions (p-refinement). For the current study, a polynomial order of $p = 6$ was employed. The treatment of spatial discretisation using the Galerkin method is well-documented by, for example, Fletcher [7,8] and Karniadakis and Sherwin [16].

In addition, the numerical method used here has been throughly verified in our works Al-Sumaily et al. [2,1], previously published for the case of forced convection heat transfer from a single cylinder embedded in a porous medium.

3.1. Resolution studies

Tests are conducted to ensure that the numerical results obtained are independent of the domain size and the spatial grid resolution. Domain size and grid resolution studies are undertaken for the configuration described in Fig. 1 for a single circular cylinder

mounted in a horizontal channel. Nu_f and Nu_s are monitored in these studies as an indicator of convergence.

3.1.1. Domain size study

The study of domain size is first performed for steady flow without pulsation. Four physical domains, i.e., $M1$, $M2$, $M3$ and $M4$, according to their upstream L_u and downstream L_d lengths from the centre of the cylinder as explained in Table 1, are chosen. The four domains are examined with and without the presence of porous media at two values of Reynolds number $Re_D = 10$ and 250, with polynomial order $p = 6$. To sufficiently resolve the higher temperature gradients near the heated cylinder the macro-element distribution is concentrated around its surface. The macro-mesh resolution is decreased in both the upstream and downstream directions to the inlet and outlet boundaries where gradients are smaller. To capture the boundary layers in the y-direction a finer mesh is employed near the walls with coarsening towards the core of the channel. The results of the study presented in Table 2, show that the $M2$ and $M3$ domains are appropriate choices for the porous and empty channels, respectively, with numerical errors less than 0.1% as measured by fluid and solid Nusselt number convergence. The distribution of the computational macro-meshes for the $M2$ and $M3$ domains are described in Fig. 2.

To use the $M2$ and $M3$ physical domains for the problem of pulsatile flow over a single cylinder inside porous and empty channels, and to ensure that they are relevant for this application, the effect of the their upstream length L_u on heat transfer from the cylinder Nu_f and Nu_s, is investigated. This investigation is done by changing the upstream length within the range of $5D_{cy} \leqslant L_u \leqslant 10D_{cy}$ for the $M2$ domain, and within $8D_{cy} \leqslant L_u \leqslant 12D_{cy}$ for the $M3$ domain. This is achieved at the highest pulsation amplitude examined, i.e., $A = 3.0$ in the porous channel, and $A = 0.7$ in the empty channel, for the lowest and highest limits of pulsation frequency $St = 0.1$ and 2.0, and for $Re_D = 1.0$ and 250. The results of the investigation are presented in Tables 3 and 4, for both channels. It is found that the $M2$ domain with $L_u = 6D_{cy}$, and the $M3$ domain with the same original upstream length $L_u = 8D_{cy}$, are appropriate for oscillatory flows in these channels with numerical errors less than 0.1%. Fig. 3 depicts the influence of L_u on the transient variation of Nu_f over one period of a pulsating flow in the porous channel, at $A = 3.0$ and $St = 0.1$, and for $Re_D = 1.0$ and 250.

3.1.2. Grid resolution study

In order to ascertain at what spectral resolution the solution becomes grid independent and subsequently which resolution provides a satisfactory compromise between accuracy and computational expense, a grid resolution study (*GRS*) for the aforementioned meshes is undertaken. As described earlier, interpolants of order $p = N - 1$ are employed to represent the solution variables throughout the spatial discretisation. This leads to a set of $N \times N$ internal node points during each macro-element of the mesh, while keeping the macro-element layout the same. Therefore, in the present study the mesh resolution is varied by changing the order of these interpolants from 2 to 8.

The *GRS* is carried out for the macro-element meshes of the $M2$ and $M3$ domains shown in Fig. 2. The *GRS* is first achieved for the porous channel, e.g., $M2$ domain, at two lowest and highest values of Reynolds number $Re_D = 1$ and 250, and at two minimum and maximum values of solid-to-fluid thermal conductivity ratio $k_r = 0.01$ and 1000. Then, the *GRS* study is done for the empty channel, e.g., $M3$ domain, at only $Re_D = 1$ and 250. Again, Nu_f and Nu_s are monitored as an indication of accuracy. The results of this case are presented in Tables 5 and 6. Here the selection of an appropriate p value relied rather on the range of p for which the solution does not diverge. These results show that Nu_f and Nu_s are converged by $p = 6$

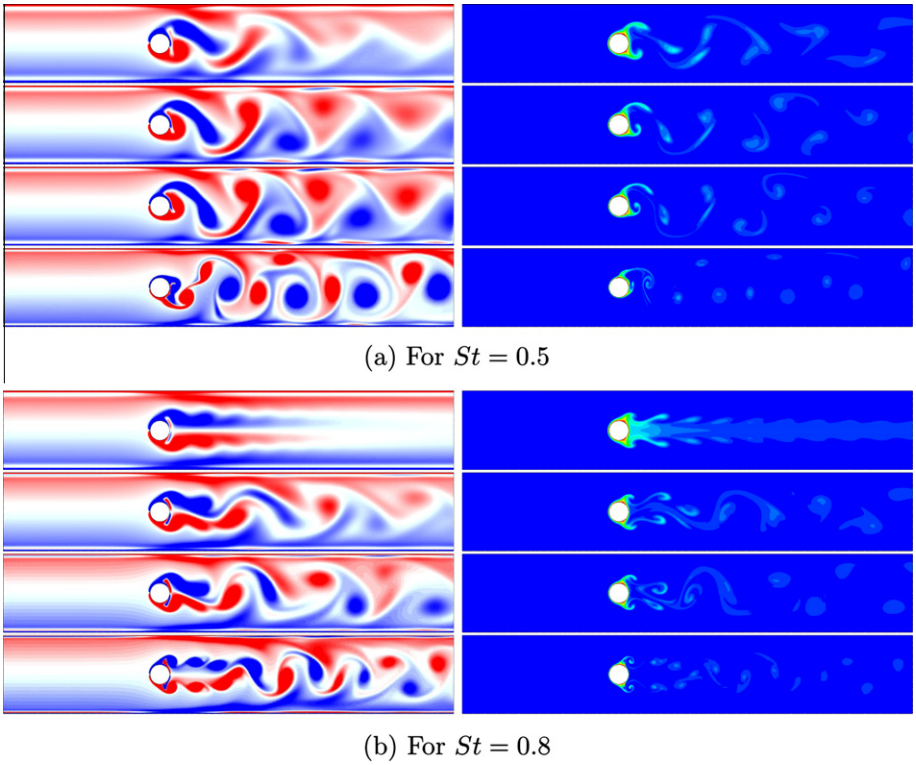

Fig. 7. Vorticity of the flow (Left) and isotherms of the thermal field around a circular cylinder placed in a horizontal empty channel exposed to a non-zero pulsatile flow, at (a) $St = 0.5$, and (b) $St = 0.8$, for different Reynolds numbers, from top to bottom, $Re_D = 40$, 70, 100 and 250, and at $A = 0.7$. Positive (negative) vorticity and hot (cold) temperatures are represented by red (blue) contours, with ranges of $(-2, 2)$ and $(0, 1)$, respectively. (For interpretation of the references to colour in this figure legend, the reader is referred to the web version of this article.)

for the porous channel, and Nu_f is converged by $p = 7$ for the empty channel, with a relative error of less than 0.5%.

The numerical simulations for the domain and mesh resolution studies have been performed at a time-step $\Delta t = 0.001$ (determined by a Courant time-step restriction), on the Monash (University) Sun Grid (*MSG*) and National Computational Infrastructure (*NCI*) high-performance computers.

4. Results and discussion

The current study presents the numerical results of forced convection heat transfer from a horizontal circular cylinder placed in a horizontal plate channel with and without the presence of porous media, under upstream steady or oscillatory flow. The main purpose of the present study is to investigate the effect of using both passive (porous media) and active (pulsation) techniques on heat transfer augmentation, and to examine the influence of pertinent pulsating flow characters, i.e., *A* and *St*, on the heat enhancement, at different porous materials.

4.1. Preliminary work

Numerical simulations were first conducted for both empty (non-filled) and porous medium filled channels to find the appropriate and possible ranges for the two key parameters *A* and *St*. In the empty channel, it was found to be not possible to obtain numerical convergence for $A > 0.7$ due to the high instability in the flow, caused by recirculations behind the cylinder, for different *St*. (This is presumably a boundary condition issue but was not pursued further.) However, for pulsating flow through a porous channel, stable behaviour resulted even for high *A* and *St*. Given this, the ranges of $A \in [0.2,3]$ and $St \in [0.1,2]$ were selected. The reason for choosing these ranges is they are higher than, and cover previously examined parameter values from the literature, and mentioned in the section *Introduction*. Also, the range for *St* in the empty channel has been chosen to be similar as that used for the porous channel studies for consistency.

Furthermore, in the porous channel, the investigation is accomplished for the following ranges of other pertinent parameters: $Re_D \in [1,250]$ and $k_r \in [0.1,100]$ which covers a wide range of

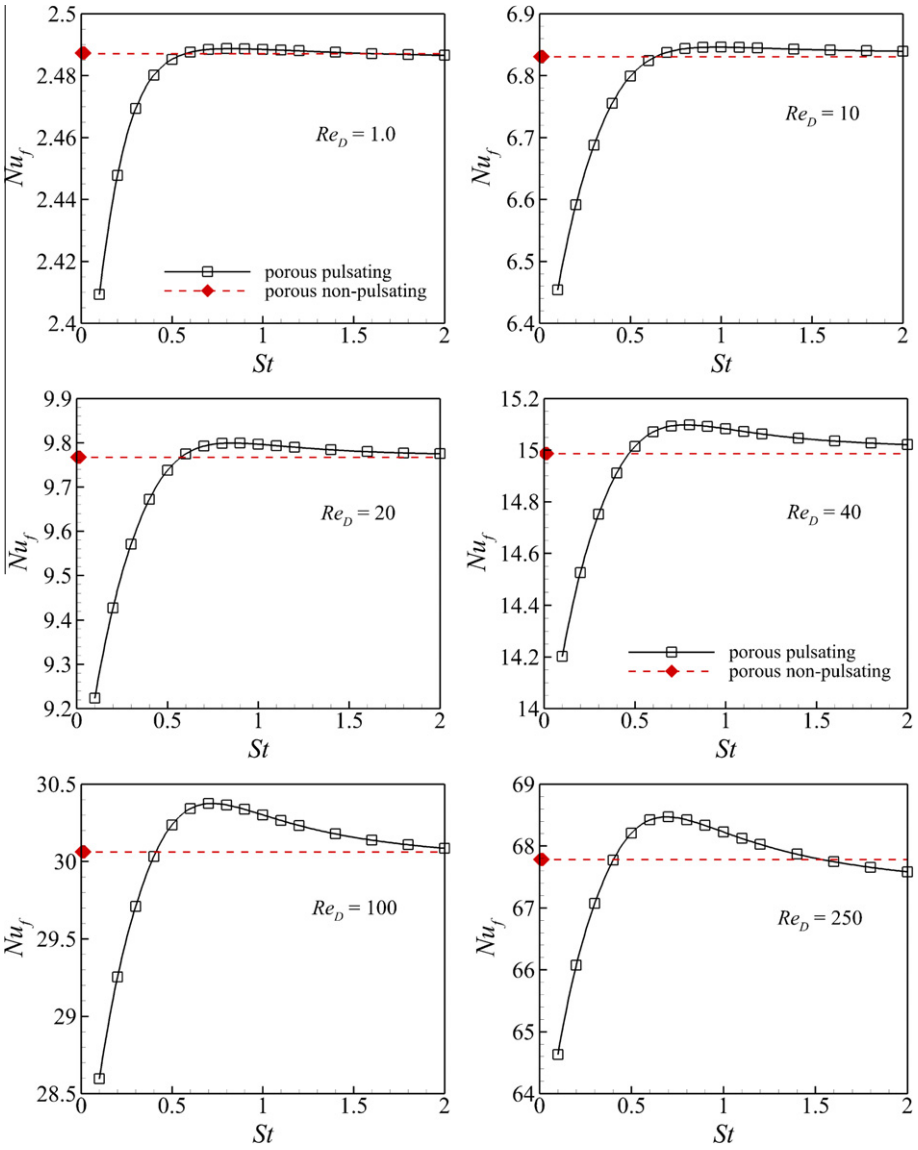

Fig. 8. Effect of the pulsation frequency represented by Strouhal number, $0.1 \leqslant St \leqslant 2.0$, on Nu_f from a cylinder immersed in a porous plate channel, for different $Re_D = 1$, 10, 20, 40, 100 and 250, at pulsation amplitude $A = 1.0$.

metallic and non-metallic porous materials with water being selected as working fluid with $k_f = 0.609$W/m K and $Pr = 7.0$. Also, this investigation is performed for the following constant values of the physical properties for the porous medium: $D_{cy}/d_p = 20$, $\varepsilon = 0.5$ and $Da = 8.333 \times 10^{-6}$. These parameter values have been chosen based both on previous studies published in the literature and to include typical combinations for physical systems. In addition, as can be seen in Eq. (10) that α_r governs only the diffusion time scales of heat within the solid phase. Therefore, α_r is held at 1.0, too.

4.2. Without the presence of porous media

4.2.1. Nusselt number

The effects of (forcing) Strouhal number, $0.1 \leqslant St \leqslant 2.0$, and amplitude $0.1 \leqslant A \leqslant 0.7$, of a non-zero pulsatile flow on the fluid Nusselt number Nu_f for the cylinder are revealed in Fig. 4. The figure displays the variation of Nu_f with St at different A, and for various values of $Re_D = 1.0$, 10, 40, 70, 100 and 250, compared with that for a steady flow. It is observed that Nu_f in pulsatile flow is smaller than that of steady flow in all conditions for $Re_D \leqslant 10$; however, Nu_f for the former flow is larger than that of the later flow for $Re_D \geqslant 40$, but the trend is not monotonic with respect to both St and A.

For $Re_D \leqslant 10$, Nu_f increases steadily as St or as A decreases. The influence of A becomes significant for lower St; however, it diminishes for high St, and visa-versa, thus the impact of St becomes considerable for higher A, and it is totally diminished at lower A.

Interestingly, for $Re_D \geqslant 40$, it is seen that the negative impact of A on Nu_f changes to the positive one, showing an increase in Nu_f as A increases. Also, the plots of Nu_f for this range of Re_D show peaks of Nu_f at a critical value of St. Below and above this critical value, Nu_f is lower. It can be also seen that the effect of A effectively vanishes at lower and higher St. In addition, the figure displays a seemingly strange behaviour of Nu_f at its peaks, where at $Re_D = 40$ and $A = 0.7$, the single peak at lower amplitudes splits into two peaks. This transition moves to lower A as Re_D increases. This behaviour may be produced from the change in the flow structure, i.e., from fully periodic to a quasi-periodic flow, at high A and a particular value of St.

4.2.2. Flow and thermal responses

The influence of external forced pulsation on the flow and temperature fields is now investigated, in an attempt to find out the reason for the *collapsed* behaviour of Nu_f as the amplitude is increased. Figs. 5 and 6 portray the flow patterns and thermal fields over two pulsation cycles at the asymptotic periodic state over eight successive phases of $2\pi t/\tau = \pi/5$, $3\pi/5$, π, $7\pi/5$, $9\pi/5$, $11\pi/5$, 3π and 4π, at $Re_D = 250$ and $A = 0.7$, and for two values of $St = 0.5$ and 0.8, marked with red circles in Fig. 4.

In these two figures, unsteady cylinder wakes are observed at both frequencies. However, the wake structure changes from fully harmonic periodic at $St = 0.8$ to sub-harmonic quasi-periodic at $St = 0.5$. In the former wake structure, the flow is shown to be symmetrically shedding and not spatio-temporally symmetric, e.g., each half is just reflection for the second half. However, in the later wake structure, a period doubling phenomenon is seen, e.g., only one half shedding cycle is shown within a one period-time. This means that the response frequency is a half of the driving pulsation frequency. In addition, the natural shedding frequency for the non-pulsating flow at $Re_D = 250$ is $\simeq$0.26. Therefore, it can be clearly seen that this phenomenon occurs at the driving pulsation frequency $St = 0.5$ which is approximately twice the natural shedding frequency. The frequency $St = 0.5$ is the frequency at which a vortex is shed from each side of the cylinder for the flow without pulsation; therefore, the inlet pulsation drives the formation of each alternating sign vortex.

In the two figures, it is obvious that the flow structure over the cylinder affects significantly its corresponding thermal response. Thus, in Fig. 5 for $St = 0.5$, it is observed that because the emerging of period doubling phenomenon due to the incomplete full cycle for the vortex shedding around the cylinder over one period, the thermal boundary layer at the rear part of the cylinder surface remains relatively large throughout the whole period-time,

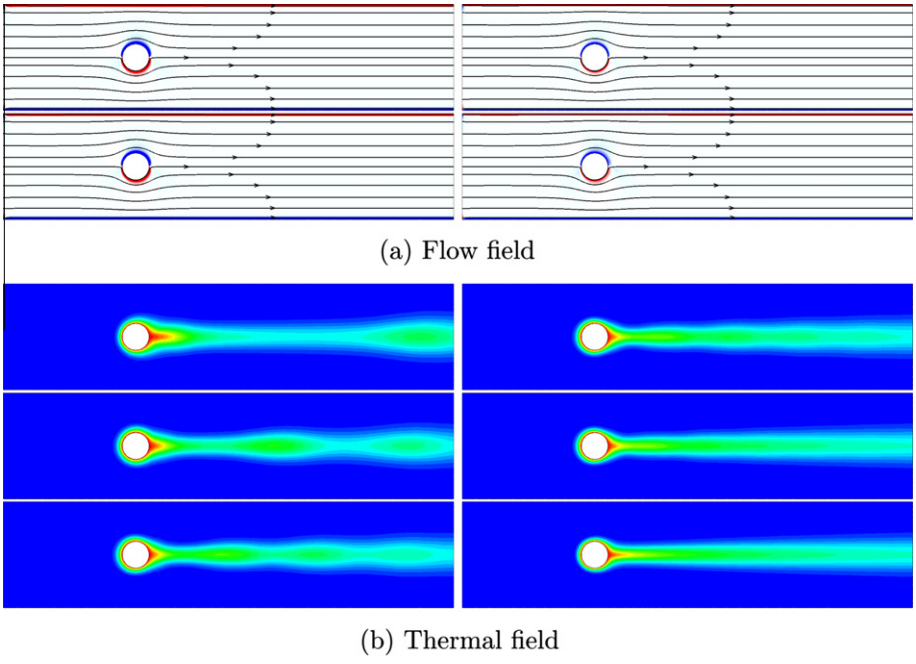

Fig. 9. (a) Vorticity with streamlines of the flow, and (b) isotherms of the thermal field, around a circular cylinder placed in a porous channel exposed to a non-zero pulsatile flow, at different pulsation frequency, from top left image and progressing first down, then across the page, (a) $St = 0.1$, 0.2, 1 and 2, and (b) $St = 0.1$, 0.2, 0.3, 0.4, 0.5 and 2, and at $Re_D = 250$ and $A = 1.0$.

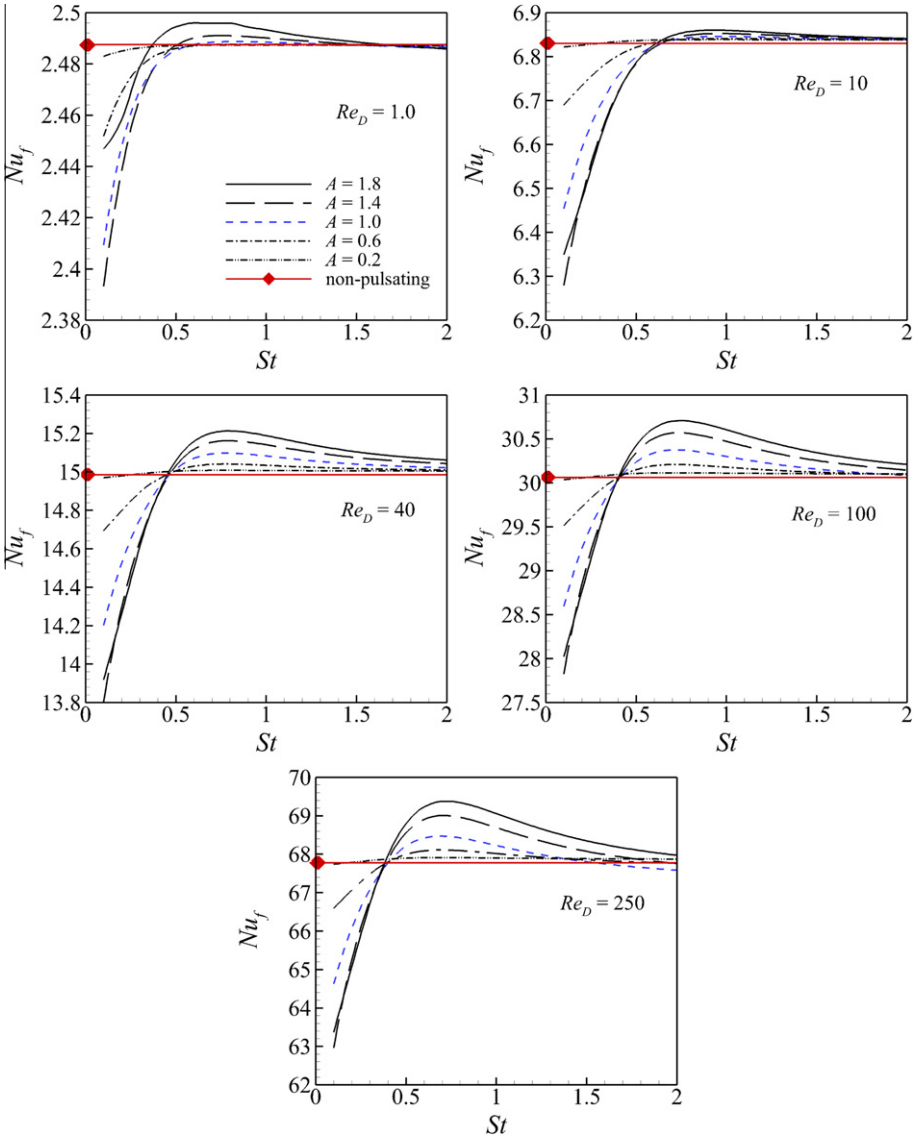

Fig. 10. The variation of Nu_f against St, for a low range of amplitude $0.2 \leqslant A \leqslant 1.8$, and for Re_D = 1, 10, 40, 100 and 250.

compared with that in Fig. 6. This reduces the temperature gradient on the hot cylinder wall and then decreases Nu_f, causing the *collapsed* behaviour of Nu_f at $St = 0.5$.

Fig. 7 displays the symmetric and non- symmetric vortex shedding that occur at $St = 0.8$ and 0.5, respectively, and their corresponding thermal fields at different Reynolds numbers $Re_D = 40$, 70, 100, 250. It is seen that at $St = 0.5$, the non-symmetric vortex shedding mode is also dominant at other different selected values of Re_D; however, the symmetric vortex shedding mode is apparent at $St = 0.8$.

4.3. In the presence of porous media

In the presence of porous media, Huang and Yang [12] have indicated the existence of a critical value of St to obtain a maximum Nu_f. This occurred at a low amplitude of $A = 0.6$. They also indicated that A has a considerable positive impact on the heat transfer enhancement at $St = 0.8$ for a Reynolds number equals to 250. Surprisingly, their results showed a negative influence from the pulsation flow on this enhancement at particular values of A and St. In addition, although, Forooghi et al. [9] found similar behaviour with respect to A at low frequencies, a different trend with a minimum value of Nu_f at a certain frequency was observed, but surprisingly the maximum Nu_f was found to occur at the lowest frequency. This case was examined at high amplitude $A = 1.5$. Therefore, the hypothesis that arises is that the trend of the variation of Nu_f with St depends on the specific values of A. Further support for this hypothesis requires further investigation over a larger amplitude range. Therefore, as mentioned in the previous section, the range used for this study $0.2 \geqslant A \geqslant 3.0$ includes those ranges previously explored in the published literature.

In this investigation, the thermal and structural properties of the porous medium used are set to fixed values as follows: solid/fluid thermal diffusivity ratio $\alpha_r = 1.0$, cylinder-to-particle diameter ratio $D_{cy}/d_p = 20$ and porosity $\varepsilon = 0.5$ with Darcy number $Da = 8.333 \times 10^{-6}$. The effect of pulsation St and A have been investigated for different metallic or non-metallic porous material, e.g., solid/fluid thermal conductivity ratio $k_r = 0.1$, 1.0, 10, 100, with water being chosen as working fluid with $k_f = 0.609$ W/m K and $Pr = 7.0$, and for Reynolds number $Re_D = 1$–250 as well. The justification and relevance of this parameter selection has been discussed previously.

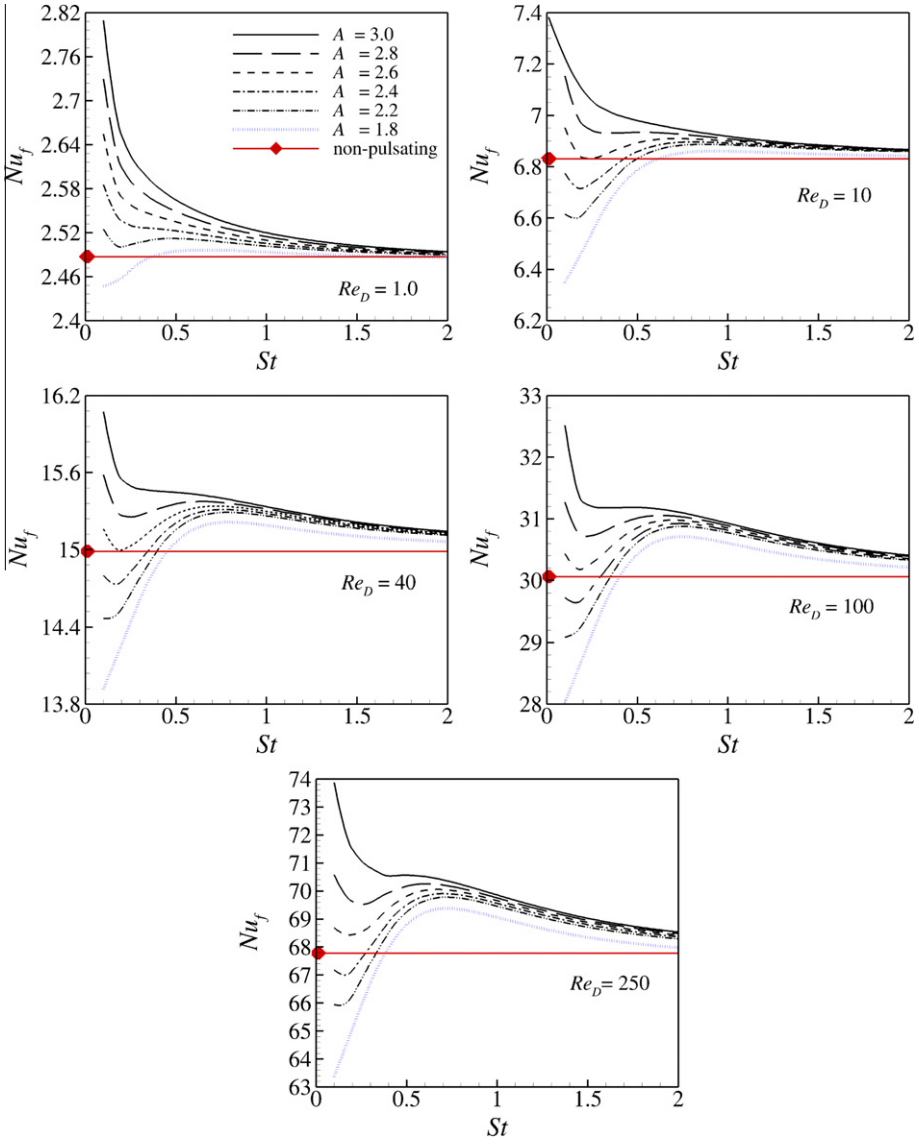

Fig. 11. The variation of Nu_f against St, for a high range of amplitude $1.8 \leqslant A \leqslant 3.0$, and for $Re_D = 1$, 10, 40, 100 and 250.

4.3.1. Effect of the pulsating frequency St

The effect of St on the cycle-averaged fluid Nusselt number distribution Nu_f is illustrated in Fig. 8, for different $Re_D = 1$, 10, 20, 40, 100 and 250, at $A = 1.0$. It can be seen that an increase in St from 0.1 to 0.7 results in a sharp increase in Nu_f, until an optimal St/heat transfer rate (around $St = 0.7$) is reached and then decreases slightly afterward. For $Re_D \leqslant 20$, the heat transfer is insensitive to the changes in the pulsating frequency when $St > 0.7$. Therefore, the peak of Nu_f is not very clear. However, this peak grows considerably and becomes very clear as Re_D increases. There are two reasons for this trend: the first reason is that increasing St causes the heat penetration distance into the fluid and the oscillation of this depth during a cycle to decrease; and the second is that the stronger oscillating interaction, caused by small eddies formed in the pores between the flowing fluid and the solid matrix in the vicinity of the heat source surface, convects more thermal energy away from the cylinder. The increasing rate of heat transfer is up to a maximum at approximately $St = 0.7$, and beyond this value it decreases due to the reduction in the above-mentioned oscillation interaction between the flow and the solid matrix near the cylinder. Nu_f for the pulsating flow is observed to be lower than that for the non-pulsating one for lower St, and for higher St but at higher Re_D. Also, it is clear that the change in Nu_f with St increases as Re_D increases.

To demonstrate the effect of variations in the pulsation frequency or Strouhal number St on the flow and thermal fields, Fig. 9 exhibits a sample of the results for $Re_D = 250$ and $A = 1.0$. It can seen that the structure of the flow fields at different St is still quite uniform, without causing recirculations in the vicinity of the cylinder. However, this effect on the thermal response throughout the channel is obviously significant, and consequently on the instantaneous thickness of thermal boundary layer around the cylinder. For example, for $A = 1.0$, the flow stops completely at a certain instantaneous time during the period time τ. For $St = 0.1$, τ is large and the flow stops only once during this period. At double the Strouhal number $St = 0.2$, there are two times when the flow instantaneously stops over the same period and so on for larger St. In consequence, as expected, the instantaneous thickness of the thermal boundary layers decreases with the increase of St from 0.1 to 0.7, while it slightly increases with an increase of the St from 0.7 to 2.

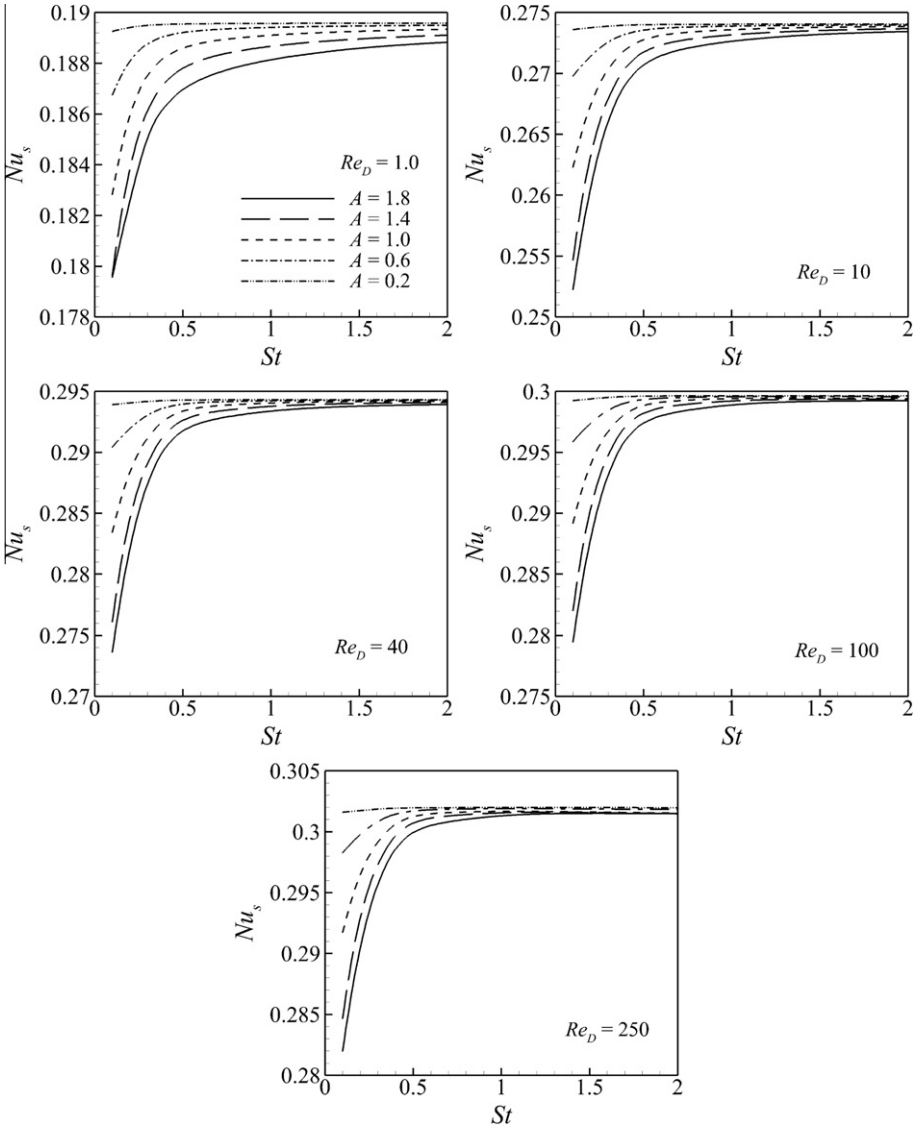

Fig. 12. The variation of Nu_s against St, for a low range of amplitude $0.2 \leqslant A \leqslant 1.8$, and for Re_D = 1, 10, 40, 100 and 250.

4.3.2. At different amplitudes

In order to look into the effects of St on heat transfer for the entire chosen range of A = 0.2–3.0 in more detail, the distributions of Nu_f and Nu_s are provided in Figs. 10–13, for five values of Re_D = 1.0, 10, 40, 100 and 250.

Fig. 10 shows the distributions of Nu_f with St for the low range of A = 0.2–1.8. Five amplitudes A = 0.2, 0.6, 1.0, 1.4 and 1.8 are selected for comparison. It is clearly seen that within this range, these distributions have the same increase–decrease profile with a peak at a certain St. The effect of St decreases as A decreases, and becomes insignificant at the lowest amplitude of A = 0.2. However, interestingly, as A increases above the value of 1.8, the initial increase with St at low St changes to a decrease from an absolute maximum, as the amplitude is increased to the maximum value examined of A = 3.0. This is shown in Fig. 11. At higher values of St > 0.5 the Nusselt number curves approach each other, relatively independent of amplitude. Between the values of A = 1.8–3.0, local minima at $St \simeq 0.2$ appear. The same qualitative trends are reported by Guo and Sung [11] in an empty tube, and by Forooghi et al. [9] in a porous channel partially filled with porous media.

More interestingly, the pulsation amplitude is shown to have a negative impact on Nu_f over its low amplitude range, i.e., A = 0.2–1.8, for low frequencies ($St \leqslant 0.5$), except for Re_D = 1.0. For that case the trend of Nu_f with St is shown not to be monotonic, and has a positive impact for high frequencies, i.e., St > 0.5. However, for the higher amplitude range, i.e., A = 1.8–3.0, this impact becomes positive for all low and high frequencies. But, the effect of A appears to be not significant at high St.

In these two Figs. 10 and 11, it is obvious that there are two ways to increase the heat transfer from hot bodies facing oscillatory cross-flows: The first way comes from the *resonance* phenomenon which happens at a certain range of oscillating amplitude A, as shown in Fig. 10, and the second way is by increasing the inlet velocity throughout increasing the pulsation amplitude A, i.e. $u_{in} = u_o + Asin(wt)$, as shown in Fig. 11. It is seen that the *resonance* phenomenon occurs at low and moderate values of amplitude A = 0.2–1.8, for getting a bill shape for Nusselt number Nu_f with a maximum value at the resonant frequency $St_{res} \approx 0.6$. However, the significant positive effect of high inlet velocity on Nu_f emerges and dominates the *resonance* phenomenon at higher A and lower pulsation frequencies St, for instance, at A = 3.0 and St = 0.1 for different values of Re_D shown in Fig. 11. The physical reason for this behaviour is that at the lowest frequency St = 0.1, each pulsation cycle takes long time period τ = 10 to be on the higher A, and

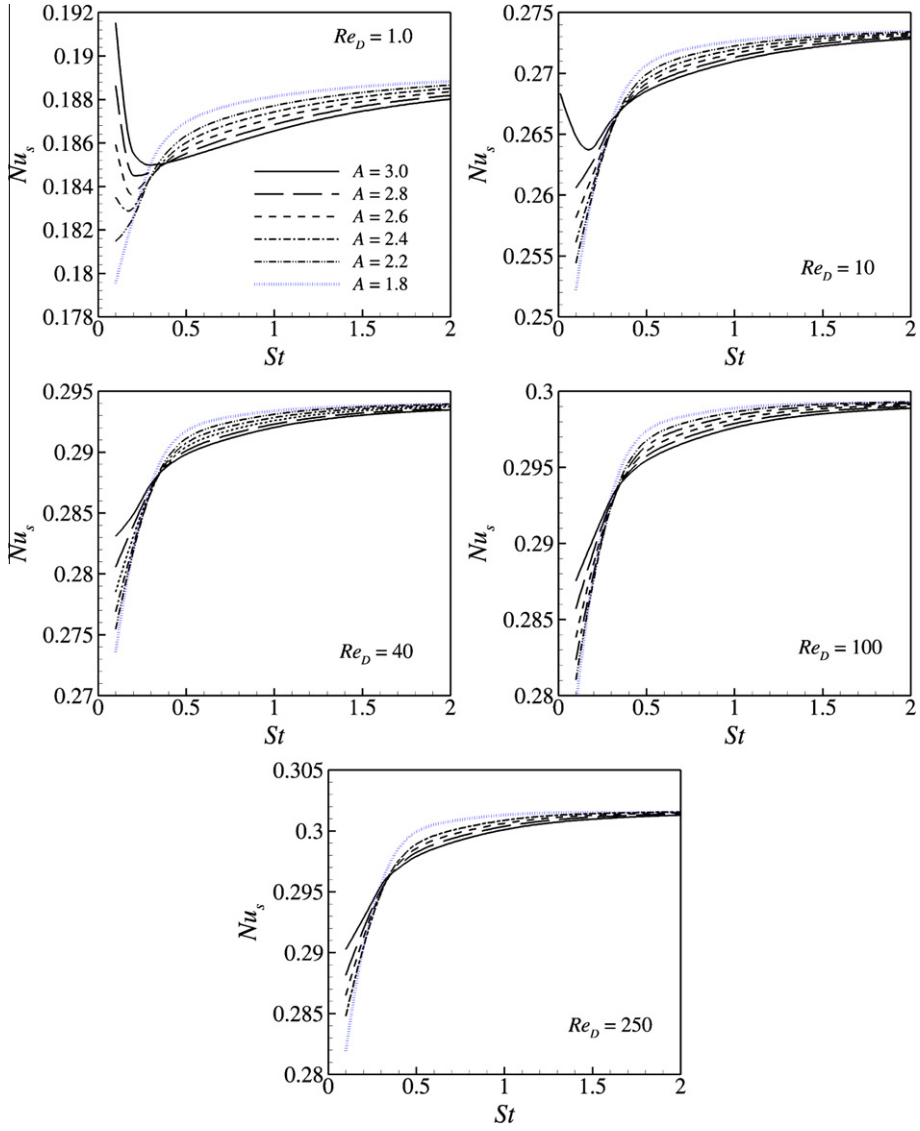

Fig. 13. The variation of Nu_s against St, for a high range of amplitude $1.8 \leqslant A \leqslant 3$, and for Re_D = 1, 10, 40, 100 and 250.

consequently thinner thermal boundary layer around the hot cylinder and then higher Nu_f. Therefore, by increasing St, the time period τ with high A becomes shorter, leading to an increase in the thickness of thermal boundary layer around the cylinder and then a decrease in Nu_f.

Furthermore, Figs. 12 and 13 present the influence of St on the variation of the cycle-average solid Nusselt number Nu_s, for different Re_D = 1, 10, 40, 100 and 250, and for the same classified low (0.2–1.8) and high (1.8–3.0) amplitude ranges previously mentioned. Firstly, the change in Nu_s with St is obviously insignificant, i.e., there is not such a change as observed for Nu_f. The plots in Fig. 12 indicate that for A = 0.2–1.8, the positive influence from St on the variation of Nu_s, especially within the range of $St \leqslant 0.7$, which seems to be the same range for gaining heat transfer within the fluid phase, decreases considerably as A decreases. Beyond this range, Nu_s becomes insensitive to the variation in St. Also, interestingly, this influence disappears completely, for all St, for A = 0.2. In addition, it is seen that Nu_s decreases as A increases for the entire range of St. However, for A = 1.8–3.0, Fig. 13 shows that the trend with A changes from a negative to a positive one, but only for low frequencies $St \leqslant 0.4$. Also, in this specific range of St and at Re_D = 1.0, it can be shown that the increasing trend of Nu_s with St changes gradually to a decreasing one, as A increases to higher values. However, this behaviour disappears as Re_D increases.

Fig. 14 shows a series of images of the fluid flow and thermal field, covering approximately one pulsation cycle, with the transient development of heat transfer in both phases. These are for the lowest pulsation frequency of St = 0.1, the highest amplitude of A = 3.0 and for Re_D = 250. These are the conditions for gaining optimal heat transfer enhancement, as shown in Fig. 11. It is clear that in spite of the fact that the value of A considered causes strong reverse flow, the flow development over time in this regime is far more stable than that for the regime without porous media. The flow varies from forward directed to backward directed, without any sign of flow recirculation either behind or in front of the cylinder. The figure demonstrates the influence of pulsation on the fluid thermal field, which responds effectively to the fluid flow.

4.4. At different porous materials

Huang and Yang [12] and Forooghi et al. [9] obtained their results for different porous materials defined by differences in the thermal conductivity of the solid. Therefore, for the present study, it is useful to investigate the effect of pulsatile flow on heat transfer

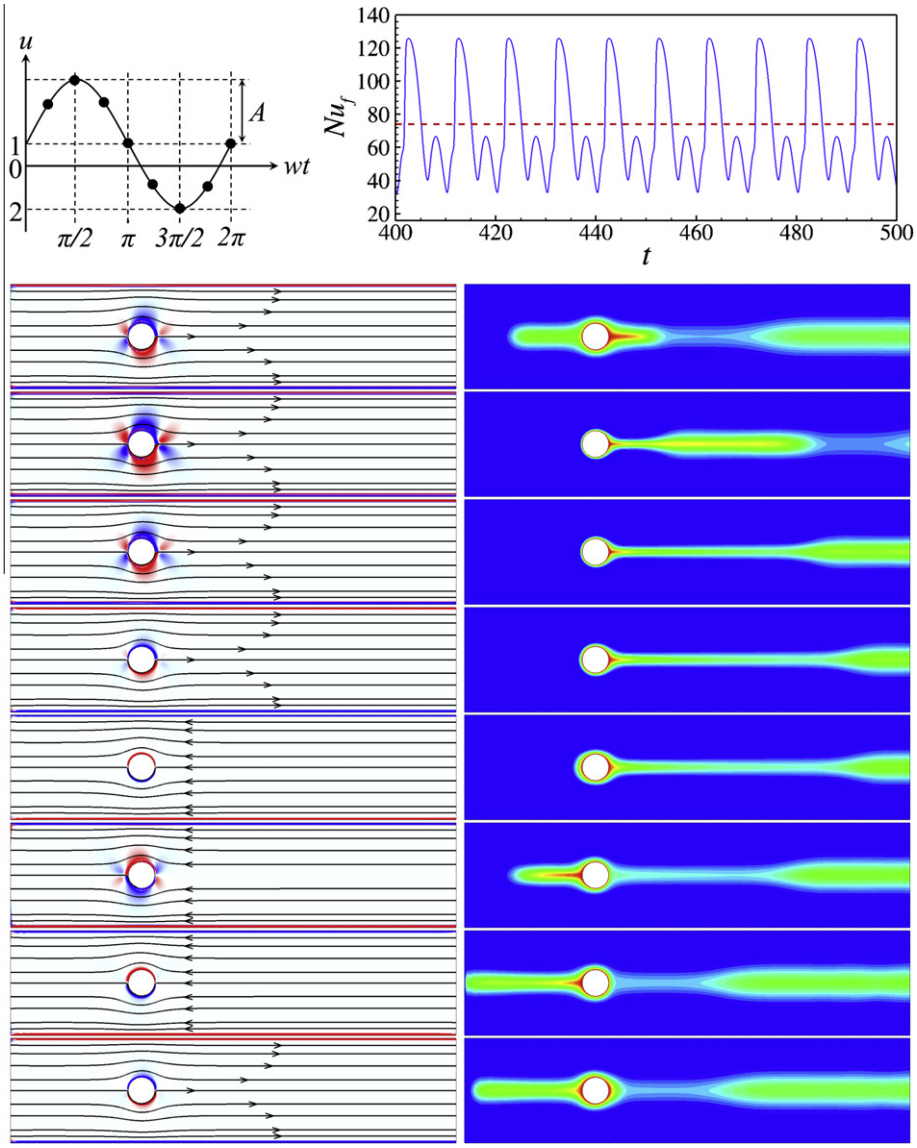

Fig. 14. Temporal fluid (Left) flow, and (Right) thermal, fields around a circular cylinder placed in a porous channel exposed to a non-zero pulsatile flow, for eight instants, from top to bottom, $wt = \pi/6$, $\pi/2$, $5\pi/6$, π, $7\pi/6$, $3\pi/2$, $11\pi/6$ and 2π, during roughly one cycle, at $St = 0.1$, $A = 3.0$ and $Re_D = 250$. The above plots represent the inlet velocity waveform (Left) and the transient behaviour of Nu_f (Right).

for different thermal conductivities corresponding to various metallic and non-metallic porous materials. Thus, Fig. 15 demonstrates the profiles of Nu_f with St for four values of $k_r = 0.1$, 1.0, 10, 100, at $A = 1.0$ and 3.0, and at $Re_D = 250$. It is clear that k_r does not have a major effect on the trend of these profiles described in the previous sections at $k_r = 1.0$ at both low and high amplitudes. Hence, Nu_f has a minimum value at the smallest St, with a maximum value at a critical St, at a *low* pulsation amplitude of $A = 1.0$. While, at *high* amplitude, for example $A = 3.0$, the profile of Nu_f changes entirely; thus, its minimum shifts to be at the largest St, and its maximum occurs at the lowest St.

In addition, it is implied that thermal conduction through the solid phase in porous media contributes to augmentation of Nu_f under pulsatile flow. However, the figure shows that this occurs only as k_r increases from 0.1 to 10, whereas the increase of k_r from 10 to 100 leads to a considerable fall in Nu_f under pulsatile forcing. This drop in Nu_f at high k_r is due to the high convective interaction between the fluid and solid phases, as clarified in our work Al-Sumaily et al. [2]. This interaction is included under the *LTNE* energy model considered in the current study.

To view the overall benefit from the application of these two techniques (passive, i.e., porous media, and/or active, i.e., pulsatile flow) for heat transfer enhancement purposes, Fig. 16 shows the variation of total average Nusselt number Nu_t with Re_D for both empty and filled channels exposed to steady inlet flow, compared with that for pulsatile inlet flow. For the empty channel, the plot corresponds to $St = 0.8$ and $A = 0.7$, which were found to be optimal values for obtaining maximum enhancement. It has been shown that a pulsating flow can lead to further enhanced thermal transport due to better fluid mixing. The value of Nu_f for pulsating inlet flow is higher than that for non-pulsating Nu_f, and the difference between them increases as Re_D increases. The higher the Re_D, the higher the convective flow acceleration (relative to diffusive forces) during the flow pulsation reversal. This leads to the production of stronger recirculation zones due to the stronger flow momentum and the smaller thickness of temporal thermal boundary layer due to the reattachment of the larger amount of core fluid to the rear part of the cylinder.

On the other hand, the optimal pulsation frequency and amplitude for gaining maximum heat transfer augmentation for the

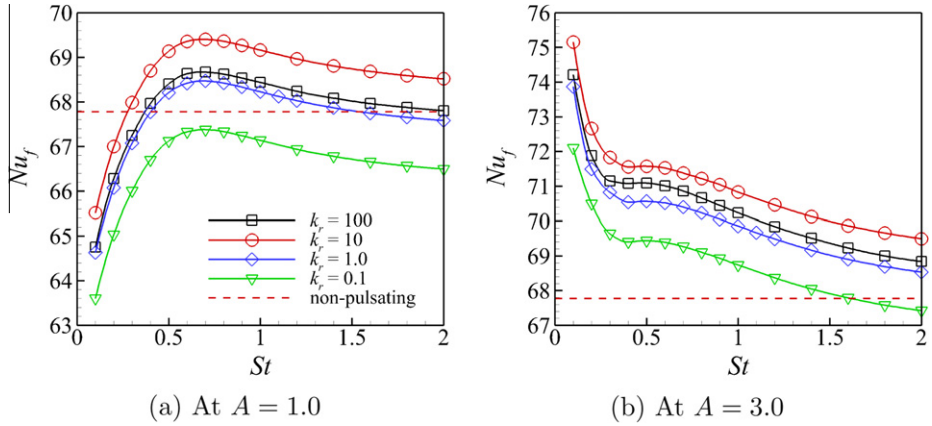

Fig. 15. The distribution of Nu_f against St, for different metallic and non-metallic porous materials, k_r = 0.1, 1.0, 10, 100, at: (a) A = 1.0 and (b) A = 3.0, and at Re_D = 250.

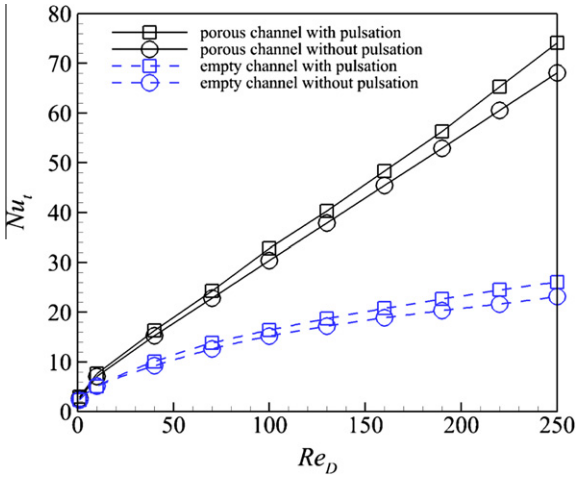

Fig. 16. Effect of a non-zero pulsatile flow on the variation of total average Nusselt number Nu_t from the heated cylinder in both empty porous channel, with Re_D. The plots of pulsatile flow are calculated as follows; in empty channel at St = 0.8 and A = 0.7, while in porous channel at St = 0.1 and A = 3.

porous case were found to be St = 0.1 and A = 3. In this figure, by comparing the plots for both channel types, it can be concluded that the passive scheme promotes a much higher heat transfer enhancement than the active one. Although, a further augmentation can be obtained by implementing pulsating inlet flow for both an empty and a porous channel, its advantage for the porous channel is more than that for the empty one, especially at higher Re_D. Indeed, it is obvious that significant benefit can be achieved from using both augmentation approaches; however, only at higher Re_D.

5. Conclusion

In this study, the influence of pulsating inlet flow on the flow and heat transfer characteristics for a heated circular cylinder within a channel in the presence and absence porous media has been explored. In particular, the effects of the control parameters, pulsation frequency St and amplitude A, are quantified, for the chosen ranges of each parameter.

Naturally, as the porous medium induces such a strong damping effect on the flow, a direct comparison with the flow and thermal behaviour for the case without a porous medium is not entirely appropriate. Despite this, the empty (non-filled) channel is used as a reference case to gauge the heat transfer augmentation possible by using porous media, and for this study, the extra enhancement from pulsatile inlet flow. In the empty channel, the unsteady cylinder wakes that evolve with the increase in Reynolds number Re_D, were observed. It was found that the wake structure changes as Re_D, A and St change. For example, at Re_D = 40 and the highest amplitude considered (A = 0.7) fully periodic vortex shedding was observed for all St, except at St = 0.5 where it changes to quasi-periodic shedding. The effect of St and A on fluid Nusselt number Nu_f depends strongly on the value of Re_D. For $Re_D \leqslant 10$, Nu_f increases as St increases and/or as A decreases. However, for $Re_D \geqslant 40$, a critical value of St was found to produce a maximum Nu_f, and the negative impact of A for lower Re_D changes to a positive one for all values of St. Interestingly, for the higher range of Re_D, there are two peaks in the Nusselt number curves at higher amplitudes, collapsing to a single peak for lower amplitudes. The collapse from two peaks to one peak occurs at increasingly lower amplitudes for higher Reynolds numbers.

For the porous-medium filled channel, the results showed a highly stable flows without the formation of extended wakes behind or in front of the cylinder, even for pulsation amplitudes which produce reverse flow in the channel. This is due to the high overall frictional damping resistance offered by the porous matrix. In the presence of porous media, Nu_f was also found to have a peak at a critical value of St. However, the results indicate that this trend is for low amplitudes A = 0.2–1.8, and it changes to a continuous decrease with Strouhal number as A is increased to higher values. These trends were established for k_r = 1.0. However, further computations for different values of k_r, characteristic of different metallic and non-metallic porous materials, i.e., k_r = 0.1, 1.0, 10, 100, showed similar trends.

Overall, the enhancement to Nu_f depends primarily on the amplitude range and then on the value of St. For instance, for A = 0.2–1.8, this effect is negative for only low frequencies, i.e., $St \leqslant 0.5$; however, it becomes positive for all St at higher amplitudes A = 1.8–3.

Generally, it can be concluded that using porous media promotes much higher heat transfer enhancement than that achievable using pulsating flow; however, this does not consider the different drag penalties associated with each. It is also obvious that the significant benefit can be obtained by combining both schemes, but only at higher Re_D.

References

[1] G.F. Al-Sumaily, A. Nakayama, J. Sheridan, M.C. Thompson, The effect of porous media particle size on forced convection from a circular cylinder without assuming local thermal equilibrium between phases, Int. J. Heat Mass Transfer 55 (2012) 3366–3378.

[2] G.F. Al-Sumaily, J. Sheridan, M.C. Thompson, Analysis of forced convection heat transfer from a circular cylinder embedded in a porous medium, Int. J. Therm. Sci. 51 (2012) 121–131.
[3] B. Alazmi, K. Vafai, Constant wall heat flux boundary conditions in porous media under local thermal non-equilibrium conditions, Int. J. Heat Mass Transfer 45 (15) (2002) 3071–3087.
[4] A.J. Chorin, Numerical solution of the Navier–Stokes equations, Math. Comput. 22 (104) (1968) 745–762.
[5] F.A. Dullien, Media Fluid Transport and Pore Structure, Academic Press, New York, 1979.
[6] S. Ergun, Fluid flow through packed columns, Chem. Eng. Prog. 48 (2) (1952) 89–94.
[7] C.A.J. Fletcher, Computational Galerkin Methods, Springer-Verlag, New York, 1984.
[8] C.A.J. Fletcher, Computational Techniques for Fluid Dynamics, vol. 1, Springer-Verlag, New York, 1991.
[9] P. Forooghi, M. Abkar, M. Saffar-Avval, Steady and unsteady heat transfer in a channel partially filled with porous media under thermal non-equilibrium condition, Transp. Porous Med. 86 (1) (2011) 177–198.
[10] K.C. Fu, X.Y. Huang, C.Y. Liu, An experimental study of heat transfer of a porous channel subjected to oscillating flow, J. Heat Transfer 123 (1) (2001) 162–170.
[11] Z. Guo, H.J. Sung, Analysis of the Nusselt number in pulsating pipe flow, Int. J. Heat Mass Transfer 40 (10) (1997) 2486–2489.
[12] P.C. Huang, C.F. Yang, Analysis of pulsating convection from two heat sources mounted with porous blocks, Int. J. Heat Mass Transfer 51 (25–26) (2008) 6294–6311.
[13] H. Iwai, T. Mambo, N. Yamamoto, K. Suzuki, Laminar convective heat transfer from a circular cylinder exposed to a low frequency zero-mean velocity oscillating flow, Int. J. Heat Mass Transfer 47 (21) (2004) 4659–4672.
[14] T.C. Jue, Analysis of flows driven by a torsionally-oscillatory lid in a fluid-saturated porous enclosure with thermal stable stratification, Int. J. Therm. Sci. 41 (8) (2002) 795–804.
[15] G.E. Karniadakis, M. Israeli, S.A. Orszag, High-order splitting methods for the incompressible Navier–Stokes equations, J. Comput. Phys. 97 (2) (1991) 414–443.
[16] G.E. Karniadakis, S.J. Sherwin, Spectral/HP Methods for Computational Fluid Dynamics, Oxford University Press, Oxford, 2005.
[17] M. Kaviany, Principles of Heat Transfer in Porous Media, Springer-Verlag, New York, 1995.
[18] J.M. Khodadadi, Oscillatory fluid flow through a porous medium channel bounded by two impermeable parallel plates, J. Fluids Eng. Trans. ASME 113 (3) (1991) 509–511.
[19] S.Y. Kim, B.H. Kang, J.M. Hyun, Heat transfer from pulsating flow in a channel filled with porous media, Int. J. Heat Mass Transfer 14 (37) (1994) 2025–2033.
[20] M. Layeghi, A. Nouri-Borujerdi, Fluid flow and heat transfer around circular cylinders in the presence and no-presence of porous media, J. Porous Med. 7 (3) (2004) 239–247.
[21] M. Layeghi, A. Nouri-Borujerdi, Darcy model for the study of the fluid flow and heat transfer around a cylinder embedded in porous media, Int. J. Comput. Methods Eng. Sci. Mech. 7 (5) (2006) 323–329.
[22] K.C. Leong, L.W. Jin, Heat transfer of oscillating and steady flows in a channel filled with porous media, Int. Commun. Heat Mass Transfer 31 (1) (2004) 63–72.
[23] K.C. Leong, L.W. Jin, An experimental study of heat transfer in oscillating flow through a channel filled with an aluminum foam, Int. J. Heat Mass Transfer 48 (2) (2005) 243–253.
[24] V.D. Murty, M.P. Camden, C.L. Clay, D.B. Paul, A study of non-Darcian effects on forced convection heat transfer over a cylinder embedded in a porous medium, in: Proceedings of the International Heat Transfer Conference, NY, USA, 1990, p. 201.
[25] D.A. Nield, A. Bejan, Convection in Porous Media, third ed., Springer Science+Business Media, New York, NY, USA, 2006.
[26] J.W. Paek, B.H. Kang, J.M. Hyun, Transient cool-down of a porous medium in pulsating flow, Int. J. Heat Mass transfer 42 (18) (1999) 3523–3527.
[27] D.A. Rees, A.P. Bassom, I. Pop, Forced convection past a heated cylinder in a porous medium using a thermal nonequilibrium model: boundary layer analysis, Eur. J. Mech. B/Fluids 22 (5) (2003) 473–486.
[28] M. Sozen, K. Vafai, Analysis of oscillating compressible flow through a packed bed, Int. J. Heat Fluid Flow 130–136 (2) (1991) 12.
[29] J. Thevenin, D. Sadaoui, About enhancement of heat transfer over a circular embedded in a porous medium, Int. Commun. Heat Mass Transfer 22 (2) (1995) 295–304.
[30] M.C. Thompson, K. Hourigan, A. Cheung, T. Leweke, Hydrodynamics of a particle impact on a wall, Appl. Math. Model. 30 (11) (2006) 1356–1369.
[31] N. Wakao, S. Kaguei, Heat and Mass Transfer in Packed Beds, Gordon and Breach, New York, 1982.
[32] N. Wakao, S. Kaguei, T. Funazkri, Effect of fluid dispersion coefficients on particle-to-fluid heat transfer coefficients in packed beds-correlation of Nusselt numbers, Chem. Eng. Sci. 34 (3) (1979) 325–336.
[33] K. Wong, N.H. Saeid, Numerical study of mixed convection on jet impingement cooling in a horizontal porous layer under local thermal non-equilibrium conditions, Int. J. Therm. Sci. 48 (5) (2009) 860–870.
[34] W.S. Wong, D.A. Rees, I. Pop, Forced convection past a heated cylinder in a porous medium using a thermal nonequilibrium model: finite Peclet number effects, Int. J. Therm. Sci. 43 (3) (2004) 213–220.
[35] L.B. Younis, Cross flowheat exchanger embedded within a porous medium, J. Porous Med. 13 (11) (2010) 981–988.
[36] L.B. Younis, A.A. Mohamad, Unsteady fluid dynamics flow and heat transfer in cross flow over a heated cylinder embedded in a porous medium, J. Porous Med. 15 (3) (2012) 203–210.
[37] P. Zehner, E.U. Schluender, Thermal conductivity of granular materials at moderate temperatures, Chemie-Ingenieur-Technik 42 (14) (1970) 933–941.